REPORT DOCUMENTATION PAGE

Form Approved OMB NO. 0704-0188

1. REPORT DATE (DD-MM-YYYY)	2. REPORT TYPE	3. DATES COVERED (From - To)
13-05-2008	Final Report	1-Apr-2005 - 31-Mar-2008

4. TITLE AND SUBTITLE

A NEW COMPUTATIONAL METHODOLOGY FOR STRUCTURAL DYNAMICS PROBLEMS

5a. CONTRACT NUMBER
W911NF-05-1-0122

5b. GRANT NUMBER

5c. PROGRAM ELEMENT NUMBER
611102

6. AUTHORS

J. N. Reddy

5d. PROJECT NUMBER

5e. TASK NUMBER

5f. WORK UNIT NUMBER

7. PERFORMING ORGANIZATION NAMES AND ADDRESSES

Texas A&M University-College Station
Administration Building, Room113
3578 TAMU
College Station, TX 77843 -3578

8. PERFORMING ORGANIZATION REPORT NUMBER

9. SPONSORING/MONITORING AGENCY NAME(S) AND ADDRESS(ES)

U.S. Army Research Office
P.O. Box 12211
Research Triangle Park, NC 27709-2211

10. SPONSOR/MONITOR'S ACRONYM(S)
ARO

11. SPONSOR/MONITOR'S REPORT NUMBER(S)
45508-EG.2

12. DISTRIBUTION AVAILIBILITY STATEMENT

Approved for Public Release; Distribution Unlimited

13. SUPPLEMENTARY NOTES

The views, opinions and/or findings contained in this report are those of the author(s) and should not contrued as an official Department of the Army position, policy or decision, unless so designated by other documentation.

14. ABSTRACT

Most structural components encountered in army vehicles and armor can be classified as beams, plates, or shells for analysis purposes. While these structural elements are designed to function properly under thermo-mechanical loads encountered in their use, they do develop high stresses and experience high vibration frequencies that may make them non-functional in actual service conditions. The objective of this research is to develop consistent plate and shell theories and associated computational framework for linear and non-linear problems of structural dynamics: (1) develop accurate and consistent structural theories and associated finite element models of plates and shells that account for transverse shear deformation

15. SUBJECT TERMS

Novel computational method, least-squares formulation, plates and shells, nonlinear analysis, FGM

16. SECURITY CLASSIFICATION OF:			17. LIMITATION OF ABSTRACT	15. NUMBER OF PAGES	19a. NAME OF RESPONSIBLE PERSON
a. REPORT	b. ABSTRACT	c. THIS PAGE			J. Reddy
U	U	U	SAR		19b. TELEPHONE NUMBER: 979-862-2417

Report Title

A NEW COMPUTATIONAL METHODOLOGY FOR STRUCTURAL DYNAMICS PROBLEMS

ABSTRACT

Most structural components encountered in army vehicles and armor can be classified as beams, plates, or shells for analysis purposes. While these structural elements are designed to function properly under thermo-mechanical loads encountered in their use, they do develop high stresses and experience high vibration frequencies that may make them non-functional in actual service conditions. The objective of this research is to develop consistent plate and shell theories and associated computational framework for linear and non-linear problems of structural dynamics: (1) develop accurate and consistent structural theories and associated finite element models of plates and shells that account for transverse shear deformation and illustrate the accuracy using benchmark plate and shell problems, and (2) develop mixed and least-squares finite element models of the refined theories for the nonlinear static and natural vibration analysis of plates and shells. Crucial importance of this framework is demonstrated computationally through well known benchmark model problems in the area of solid mechanics with special focus on composite structures. The developed methodology and the resulting infrastructure with its applications to solid and structural mechanics problems should provide highly reliable, robust and accurate computational technology to the United States Army Laboratories.

List of papers submitted or published that acknowledge ARO support during this reporting period. List the papers, including journal references, in the following categories:

(a) Papers published in peer-reviewed journals (N/A for none)

• J.N. Reddy and R. A. Arciniega, “Mechanical and Thermal Buckling of Ceramic-Metal Plates,” Chapter 6 in Analysis and Design of Plated Structures, Statics, N. E. Shanmugam and C. M. Wang (eds), Wood-Head Publishing, Oxford, UK, pp. 138-160, 2005.

• R. A. Arciniega and J. N. Reddy, “A Consistent Third-Order Shell Theory with Application to Bending of Laminated Composite Cylindrical Shells,” AIAA Journal, Vol. 43, No. 9, pp. 2024-2038, 2005.

• V. Prabhakar and J. N. Reddy, “Spectral/hp Penalty Least-Squares Finite Element Formulation for the Steady Incompressible Navier-Stokes Equations,” Journal of Computational Physics, Vol. 215, No. 1, pp. 274-297, 2006.

• J.N. Reddy and R. A. Arciniega, “Vibration of Functionally Graded Ceramic-Metal Plates,” in Analysis and Design of Plated Structures: Dynamics, N. E. Shanmugam and C. M. Wang (eds), Wood-Head Publishing, Oxford, UK, pp. 293-321, 2007.

• R. A. Arciniega and J. N. Reddy, “Tensor-based Finite Element Formulation for Geometrically Nonlinear Analysis of Shell Structures,” Computer Methods in Applied Mechanics and Engineering, Vol. 196, Nos. 4-6, pp. 1048-1073, 2007.

• R. A. Arciniega and J. N. Reddy, “Large deformation analysis of functionally graded shells,” International Journal of Solids and Structures, Vol. 44, pp. 2036-2052, 2007.

• V. Prabhakar and J. N. Reddy, "A Stress-based Least-Squares Finite-element model for Incompressible Navier-Stokes Equations," International Journal for Numerical Methods in Fluids, vol. 54, issue 11, pp. 1369-1385, 2007.

• F. Moleir, C.M. Mota Soares, C.A. Mota Soares, and J.N. Reddy, “Mixed least-squares finite element model for the static analysis of laminated composite plates,” Computers and Structures, Vol. 86 pp. 826–838, 2008.

• Henrique Santos, C. M. Mota Soares, C. A. Mota Soares, and J.N. Reddy, “A finite element model for the analysis of 3D axisymmetric laminated shells with piezoelectric sensors and actuators: Bending and free vibrations,” Computers and Structures, Vol. 86 pp. 940–947, 2008.

Number of Papers published in peer-reviewed journals: 9.00

(b) Papers published in non-peer-reviewed journals or in conference proceedings (N/A for none)

J. N. Reddy, “Linear and Nonlinear Analysis of Shells,” Lecture delivered at the Workshop on Computational Methods in Structural Mechanics and Fluid Flows (COSMECFLOWS), Osmania University, Hyderabad, India, December 5, 2005.

J. N. Reddy, “A Finite Deformation Shell Formulation for the Analysis of Composite and Functionally Graded Material Structures,” Invited Lecture presented at Symposium on Physics and Mechanics of Advanced Materials, January 18-20, 2006, Singapore.

J. N. Reddy, “A Consistent Finite Element Model for Nonlinear Analysis of Composite and Functionally Graded Shell Structures,” Opening Plenary Lecture presented at International Conference on Composite Materials and Nano-Structures (IC2MS-06), April 26-29, 2006, Shah Alam (Kaula Lumpur), Malaysia.

J. N. Reddy, “Nonlinear Analysis of Composite and FGM Shell Structures Using Tensor-Based Shell Elements,” III European Conference on Computational Mechanics, Solids, Structures and Coupled Problems in Engineering, LNEC, Lisbon, Portugal, June 5-8, 2006.

F. Moleiro, C. M. Mota Soares, C. A. Mota Soares, J. N. Reddy,“Mixed Finite Elements based on Least-Squares Formulation for the Static Analysis of Laminated Composite Plates,” III European Conference on Computational Mechanics, Solids, Structures and Coupled Problems in Engineering, LNEC, Lisbon, Portugal, June 5-8, 2006.

J. N. Reddy, “Nonlinear Analysis of Functionally Graded Shell Structures Using Tensor-Based Shell Element,“ Key Note Lecture, 5th International Conference on Mechanics and Materials in Design (M2D’2006), Porto, Portugal, July 24-26, 2006.

J. N. Reddy, “On Nonlinear Analysis of Composite and Functionally Graded Shell Structures,” Invited Lecture, Tenth East Asia Pacific Conference on Structural Engineering and Construction, August 2-4, 2006, Bangkok, Thailand.

J. N. Reddy, “Computational Models of Viscous Flows and Shell Structures,” Invited Lecture presented at International Conference on Enhancement and Promotion of Computational Methods in Engineering Science and Mechanics (CMESM 2006), Changchun, China, August 10-12, 2006.

J. N. Reddy, “Tensor-Based Shell Element and Modeling of Biological Cells,” Plenary Lecture, the International Conference on Recent Developments in Structural Engineering (RDSE-2007), Manipal Institute of Technology, Manipal, India, 30 August – 1 September, 2007.

J. N. Reddy, “A First-Order Shell Theory with Thickness Stretch and Locking-Free Shell Finite Element,” Opening Plenary Lecture and (and Chief Guest), International Conference on Computer Aided Engineering, December 13-16, 2007, Indian Institute of Technology-Madras, Chennai, India.

Number of Papers published in non peer-reviewed journals: 9.00

(c) Presentations

J. N. Reddy,“Nonlinear Analysis of Composite and FGM Shell Structures Using Tensor-Based Shell Elements,” International Workshop in Mechanics of Composites, Bad Herrenab, Germany, November 26-29, 2006.

J. N. Reddy, “The Finite Element Method in Structures and Beyond,” SPDC ASME USB (Student Professional Development Conference), University of Simon Bolivar, Caracas, Venezuela, May 9-13, 2007.

V. Prabhakar and J. N. Reddy, “Least-squares Based Finite Element Formulations for Newtonian and non-Newtonian Fluid Flows,” paper presented in Computational Methodologies for Navier-Stokes and Turbulence session, at McMat 2007, ASME Applied Mechanics and Materials Conference, June 3-7, 2007, University of Texas at Austin, Austin, Texas.

Number of Presentations: 3.00

Non Peer-Reviewed Conference Proceeding publications (other than abstracts):

Number of Non Peer-Reviewed Conference Proceeding publications (other than abstracts): 0

Peer-Reviewed Conference Proceeding publications (other than abstracts):

Number of Peer-Reviewed Conference Proceeding publications (other than abstracts): 0

(d) Manuscripts

Number of Manuscripts: 0.00

Number of Inventions:

Graduate Students

NAME	PERCENT_SUPPORTED
Roman Arciniega	0.50
Vivek Prabhakar	0.50
Yetzirah Urthaler	0.50
FTE Equivalent:	**1.50**
Total Number:	**3**

Names of Post Doctorates

NAME	PERCENT_SUPPORTED
Roman Arciniega	0.50
FTE Equivalent:	**0.50**
Total Number:	**1**

Names of Faculty Supported

NAME	PERCENT_SUPPORTED	National Academy Member
J. N. Reddy	0.25	No
FTE Equivalent:	**0.25**	
Total Number:	**1**	

Names of Under Graduate students supported

NAME	PERCENT_SUPPORTED
FTE Equivalent:	
Total Number:	

Student Metrics

This section only applies to graduating undergraduates supported by this agreement in this reporting period

The number of undergraduates funded by this agreement who graduated during this period:	0.00
The number of undergraduates funded by this agreement who graduated during this period with a degree in science, mathematics, engineering, or technology fields:.....	0.00
The number of undergraduates funded by your agreement who graduated during this period and will continue to pursue a graduate or Ph.D. degree in science, mathematics, engineering, or technology fields:.....	0.00
Number of graduating undergraduates who achieved a 3.5 GPA to 4.0 (4.0 max scale):	0.00
Number of graduating undergraduates funded by a DoD funded Center of Excellence grant for Education, Research and Engineering:	0.00
The number of undergraduates funded by your agreement who graduated during this period and intend to work for the Department of Defense	0.00
The number of undergraduates funded by your agreement who graduated during this period and will receive scholarships or fellowships for further studies in science, mathematics, engineering or technology fields:	0.00

Names of Personnel receiving masters degrees

NAME
Brittan Pratt
Total Number: 1

Names of personnel receiving PHDs

NAME
Roman Arciniega
Vivek Prabhakar
Yetzirah Urthaler
Total Number: 3

Names of other research staff

NAME	PERCENT_SUPPORTED
FTE Equivalent:	
Total Number:	

Sub Contractors (DD882)

Inventions (DD882)

A NEW COMPUTATIONAL METHODOLOGY FOR STRUCTURAL DYNAMICS PROBLEMS

J. N. Reddy
Department of Mechanical Engineering
Texas A&M University
College Station, Texas 77843-3123
e-mail: jnreddy@tamu.edu

ARO Grant W911NF-05-1-0122
AMSRD-ARL-RO-OI Proposal Number: 45508-EG

Final Technical Report
submitted to

U. S. Army Research Office
P.O. Box 12211
Research Triangle Park, NC 27709-2211

April 2008

TABLE OF CONTENTS

A NEW COMPUTATIONAL METHODOLOGY FOR STRUCTURAL DYNAMICS PROBLEMS

ARO Grant W911NF-05-1-0122
AMSRD-ARL-RO-OI Proposal Number: 45508-EG

J. N. Reddy
Department of Mechanical Engineering
Texas A&M University

EXECUTIVE SUMMARY

Most structural components encountered in army vehicles and armor can be classified as beams, plates, or shells for analysis purposes. While these structural elements are designed to function properly under thermo-mechanical loads encountered in their use, they do develop high stresses and experience high vibration frequencies that may make them non-functional in actual service conditions. The objective of this research is to develop consistent plate and shell theories and associated computational framework for linear and non-linear problems of structural dynamics in which localized high gradients of the solutions are resolved accurately and time accuracy of the solution is assured at all stages during the evolution. Crucial importance of this framework will be demonstrated computationally through well known benchmark model problems in the area of solid mechanics with special focus on composite structures. The developed methodology and the resulting infrastructure with its applications to solid and structural mechanics problems should provide highly reliable, robust and accurate computational technology to the United States Army Laboratories. The specific objectives of this research were:

- Develop accurate and consistent structural theories and associated finite element models of plates and shells that account for transverse shear deformation and illustrate the accuracy using benchmark plate and shell problems.
- Develop mixed and least-squares finite element models of the refined theories for the analysis of plates and shells.

In the following pages a technical discussion of the scientific progress made and accomplishments are summarized in two parts:

1. A robust shell finite element for nonlinear analysis of composite and functionally graded shells, and
2. Mixed least-squares finite element models for bending and vibration of plates.

1. LARGE DEFORMATION ANALYSIS OF SHELLS

1.1 Introduction

Composite shells have been of great interest in many engineering applications. Composites made up of fiber-reinforced laminae that are bonded together (Reddy, 2004) are particularly attractive. A typical lamina is often characterized as orthotropic with the principal material directions of each lamina coinciding with the fiber direction and transverse to it. As required in a design, by changing the material type, fiber orientation, or thickness, the designer can tailor the different properties of a laminate to suit a particular application. Despite their multiples advantages, laminated composites exhibit a serious shortcoming due to concentrations of stresses, as well as in-surface displacements, caused by the piece-wise variation of the material properties through the thickness of the shell. Consequently, a special material named "functionally graded materials" (FGMs) was proposed by Koizumi (1997) and Yamanouchi et al. (1990), in which the material properties vary smoothly and continuously from one surface to the other. These materials are inhomogeneous and made from isotropic components. The gradation of the material properties through the thickness avoids jumps or abrupt changes on the stress and displacement distributions of any thin-walled structure.

In some applications shell structures can experience large elastic deformations and finite rotations. Geometric nonlinearity plays an essential role in the behavior of the shell, especially when it reaches large deformations. Previous studies show that laminated shells exhibit drastic changes in their bending response (Başar et al.,1993; Vu-Quoc and Tan, 2003; Balah and Al-Ghamedy, 2002). Even for homogeneous and isotropic shells we observe an unpredictable behavior (Simo et al., 1990; Sansour and Kollmann, 2000). Therefore, it is of vital importance to study the nonlinear response of potentially inhomogeneous materials such as functionally graded shells.

This paper is motivated by the lack of studies found in the literature that addresses large deformation analysis for FGM shells. A review of technical articles shows that few studies have been carried out to investigate the nonlinear bending response of plates and shells. Most of them use von Kármán or Sanders theories which are restricted to moderately small deformations. We cite the papers of Na and Kim (2005), who examined the effect of thermal loading and uniform pressure on the bending response of FGM plates; and Yang and Shen (2003a,b), who analyzed the nonlinear bending and postbuckling behavior for FGM plates under thermomechanical load with various boundary conditions. Woo and Meghid (2001) provided an analytical solution for large deflection FGM plates and shells under mechanical and thermal loading; while Ma and Wang (2003) examined the axisymmetric large deflection bending and thermal postbuckling of FGM circular plates subjected to mechanical and thermal loading. Both articles are based on the classical von Kármán plate theory.

Moreover, Reddy and Chin (1998) analyzed the dynamic thermoelastic response of functionally graded cylinders and plates. Praveen and Reddy (1998) carried out a nonlinear thermoelastic analysis of functionally graded ceramic-metal plates using a finite element model based on the FSDT. Thermomechanical buckling, as well as bending and free vibration analysis, of FGM plates can be found in the articles by Reddy and Arciniega (2006a,b). Further studies of bending and vibration analyses of FGMs plates can be found in the articles of Reddy (2000), and Della Croce and Venini (2004).

On the subject of computational models for shell structures, we focus our attention on tensor-based finite element models (Harte and Eckstein, 1986). This approach is able to determine all properties of the shell's differential geometry exactly. Additional errors, introduced by approximating the geometry of the midsurface of the shell (as in continuum-based finite element models), are prevented from the beginning. Previous works of the authors using tensor-oriented finite element formulations for linear analysis of laminated shells can be found in Arciniega and Reddy (2005), and Reddy and Arciniega (2004).

In this paper, a large deformation analysis for functionally graded shells is presented. The formulation is based on the first-order shear deformation theory with seven independent parameters (Sansour, 1995; Bischoff and Ramm, 1997) where no plane stress assumption is required (3D constitutive equations). A tensor-based finite element model is developed using high-order Lagrange elements to preclude membrane shear locking. The gradation of the material properties of the FGM shell is considered through the thickness. The material stiffness tensor is obtained by Gauss integration. Numerical results are presented for typical benchmark problems with applications to functionally graded shells.

1.2. Theoretical Formulation

The shell theory will be briefly discussed here. For a detailed development, one can consult the paper of Arciniega and Reddy (2006) and references herein. The mathematical background utilized in the following derivation is given in the books of Naghdi (1963) and (1972), Green and Zerna (1968), and Pietraszkiewicz (1979).

Let us introduce in the region $\mathsf{B}_R(\mathsf{B}_t)$ a *convected* curvilinear coordinate system $\{\theta^i\}$, $i=1,2,3$, such that the surface $\theta^3=0$ defines the midsurface $\mathsf{M}_R(\mathsf{M}_t)$ of the region $\mathsf{B}_R(\mathsf{B}_t)$. The coordinate θ^3 is the measure of the distance between points $P\in\mathsf{B}_R$ $(\bar{P}\in\mathsf{B}_t)$ and $M\in\mathsf{M}_R$ $(\bar{M}\in\mathsf{M}_t)$, with $-h/2\le\theta^3\le h/2$, where h is the thickness of the shell (Fig. 1).

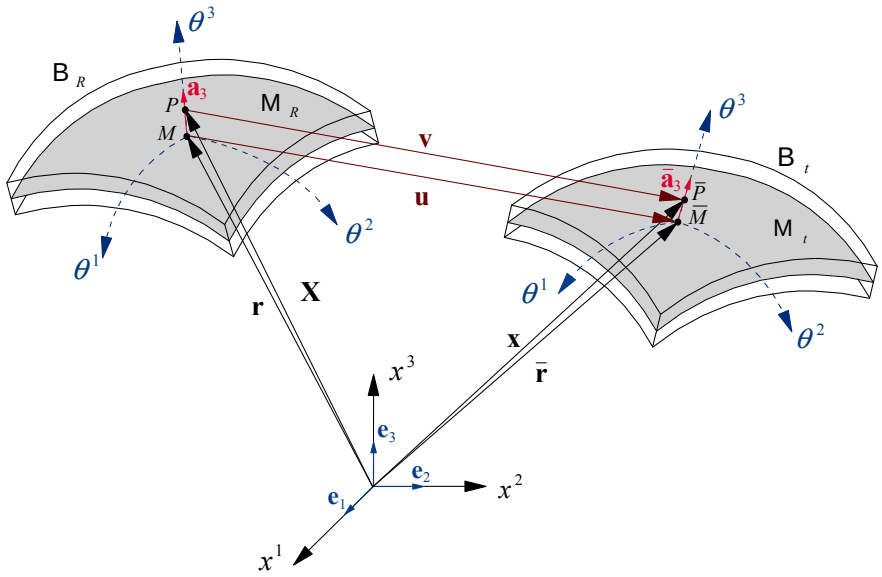

Fig. 1. Shell continuum in the reference and current configurations.

Consider the motion $\chi(\mathbf{X},t)$ of the shell body B from the reference configuration B_R to the current configuration B_t. Since a convected coordinate system $\{\theta^i\}$ has been adopted, geometric quantities of the region B_t are analogous to those defined in B_R. In the Lagrangian description, the displacement of the particle X from the reference configuration to the current configuration is given by the vector $\mathbf{v}(\mathbf{X},t)$, i.e.

$$\begin{aligned}\mathbf{v}(\mathbf{X},t) &= \chi(\mathbf{X},t) - \mathbf{X} = \mathbf{x} - \mathbf{X} \\ &= V^i \mathbf{g}_i = V_j \mathbf{g}^j\end{aligned} \tag{1}$$

wherein the last line is in component form with respect to the region B_R.

We introduce the first kinematical assumption for the shell model: "the displacement field is considered as a linear expansion of the thickness coordinate around the midsurface. The transverse displacement is parabolic through the thickness of the shell".

This assumption implies that

$$\mathbf{v}(\theta^\alpha) = \mathbf{u}(\theta^\alpha) + \theta^3 \boldsymbol{\varphi}(\theta^\alpha) \underline{+(\theta^3)^2 \underline{\boldsymbol{\Psi}}(\theta^\alpha)} \tag{2}$$

where

$$\mathbf{u}(\theta^\alpha) = u_i \mathbf{a}^i, \quad \boldsymbol{\varphi}(\theta^\alpha) = \varphi_i \mathbf{a}^i, \quad \underline{\boldsymbol{\Psi}}(\theta^\alpha) = \psi_3 \mathbf{a}^3 \tag{3}$$

The underlined term of equation (2) is included to avoid Poisson locking (Bischoff and Ramm, 1997).

The position vector of the deformed shell can be obtained substituting equation (2) into (1). Thus

$$\mathbf{x} = \bar{\mathbf{r}} + \theta^3 \bar{\mathbf{a}}_3 + (\theta^3)^2 \underline{\boldsymbol{\Psi}} \tag{4}$$

where $\bar{\mathbf{r}} = \mathbf{r} + \mathbf{u}$ and $\bar{\mathbf{a}}_3 = \mathbf{a}_3 + \boldsymbol{\varphi}$. The vector $\boldsymbol{\varphi}$ is also called difference vector (change of the director of the midsurface). The director $\bar{\mathbf{a}}_3$ is, in general, neither a unit vector nor orthogonal to M_t. The configuration of the shell is uniquely determined by the displacement vector $\mathbf{u}$ of the midsurface together with the difference vector $\boldsymbol{\varphi}$ and the additional variable $\underline{\boldsymbol{\Psi}}$, or by seven independent components of these vectors (Sansour, 1995).

We now introduce the Green strain tensor $\mathbf{E}$ as a measure of the strain for a material description

$$\mathbf{E} = \frac{1}{2}(\mathbf{C} - \mathbf{G}) \tag{5}$$

where $\mathbf{C} = \mathbf{F}^T \mathbf{F}$ is the *right Cauchy-Green tensor*, $\mathbf{G} = g_{ij} \mathbf{g}^i \otimes \mathbf{g}^j$ is *the Riemannian metric* in the reference configuration and $\mathbf{F} = \bar{\mathbf{g}}_i \otimes \mathbf{g}^i$ is the deformation gradient. We define the covariant space and surface base vectors in the current configuration as $\bar{\mathbf{g}}_i$ and $\bar{\mathbf{a}}_i$, respectively.

The shifter tensor $\boldsymbol{\mu}$ is a two-point tensor which relates the region B_R to the reference midsurface M_R and it is useful to define the tensor $\hat{\mathbf{E}}$ as

$$\hat{\mathbf{E}} = \Phi^*\left(\mathbf{E}\right) = \boldsymbol{\mu}^T \mathbf{E}\, \boldsymbol{\mu} \tag{6}$$

where $\Phi^*\left(\circ\right)$ is the pull-back operator.

The tensor $\hat{\mathbf{E}}$ can be expanded as a function of the thickness coordinate, i.e.

$$\hat{\mathbf{E}} = \boldsymbol{\varepsilon}^0 + \theta^3 \boldsymbol{\varepsilon}^1 \underline{+ (\theta^3)^2 \boldsymbol{\varepsilon}^2 + (\theta^3)^3 \boldsymbol{\varepsilon}^3 + (\theta^3)^4 \boldsymbol{\varepsilon}^4} \tag{7}$$

The second assumption for the shell model asserts that: "quadratic and higher-order terms of $\hat{\mathbf{E}}$, underlined in equation (7), are negligible". Then, we arrive to the following decomposition

$$\begin{aligned} \boldsymbol{\varepsilon}^0 &= \varepsilon^{(0)}_{\alpha\beta}\, \mathbf{a}^\alpha \otimes \mathbf{a}^\beta + \varepsilon^{(0)}_{\alpha 3} (\mathbf{a}^\alpha \otimes \mathbf{a}^3 + \mathbf{a}^3 \otimes \mathbf{a}^\alpha) + \varepsilon^{(0)}_{33} \mathbf{a}^3 \otimes \mathbf{a}^3 \\ \boldsymbol{\varepsilon}^1 &= \varepsilon^{(1)}_{\alpha\beta}\, \mathbf{a}^\alpha \otimes \mathbf{a}^\beta + \varepsilon^{(1)}_{\alpha 3} (\mathbf{a}^\alpha \otimes \mathbf{a}^3 + \mathbf{a}^3 \otimes \mathbf{a}^\alpha) + \varepsilon^{(1)}_{33} \mathbf{a}^3 \otimes \mathbf{a}^3 \end{aligned} \tag{8}$$

where $\varepsilon^{(i)}_{\alpha\beta}, \varepsilon^{(i)}_{\alpha 3}$ and $\varepsilon^{(i)}_{33}$ are functions of the triple $\left(\mathbf{u}, \boldsymbol{\varphi}, \underline{\boldsymbol{\Psi}}\right)$. After some manipulations we can write them in terms of the seven components of the displacement field (Habip, 1965), i.e.

$$\begin{aligned} \varepsilon^{(0)}_{\alpha\beta} &= \frac{1}{2}\Big(u_{\alpha|\beta} + u_{\beta|\alpha} - 2b_{\alpha\beta}u_3 + a^{\lambda\gamma}u_{\lambda|\alpha}u_{\gamma|\beta} - b^\lambda_\beta u_3 u_{\lambda|\alpha} - b^\lambda_\alpha u_3 u_{\lambda|\beta} \\ &\quad + c_{\alpha\beta}(u_3)^2 + u_{3,\alpha}u_{3,\beta} + b^\lambda_\alpha u_\lambda u_{3,\beta} + b^\lambda_\beta u_\lambda u_{3,\alpha} + b^\lambda_\alpha b^\gamma_\beta u_\lambda u_\gamma\Big) \\ \varepsilon^{(1)}_{\alpha\beta} &= \frac{1}{2}\Big(\varphi_{\alpha|\beta} + \varphi_{\beta|\alpha} - 2b_{\alpha\beta}\varphi_3 - b^\lambda_\beta u_{\lambda|\alpha} - b^\lambda_\alpha u_{\lambda|\beta} + 2c_{\alpha\beta}u_3 + a^{\lambda\gamma}u_{\lambda|\alpha}\varphi_{\gamma|\beta} \\ &\quad + a^{\lambda\gamma}u_{\lambda|\beta}\varphi_{\gamma|\alpha} - b^\lambda_\beta\varphi_3 u_{\lambda|\alpha} - b^\lambda_\alpha\varphi_3 u_{\lambda|\beta} - b^\lambda_\beta u_3\varphi_{\lambda|\alpha} - b^\lambda_\alpha u_3\varphi_{\lambda|\beta} + 2c_{\alpha\beta}u_3\varphi_3 \\ &\quad + u_{3,\alpha}\varphi_{3,\beta} + u_{3,\beta}\varphi_{3,\alpha} + b^\lambda_\alpha\varphi_\lambda u_{3,\beta} + b^\lambda_\beta\varphi_\lambda u_{3,\alpha} + b^\lambda_\alpha u_\lambda\varphi_{3,\beta} + b^\lambda_\beta u_\lambda\varphi_{3,\alpha} \\ &\quad + b^\lambda_\alpha b^\gamma_\beta u_\lambda\varphi_\gamma + b^\lambda_\beta b^\gamma_\alpha u_\lambda\varphi_\gamma\Big) \\ \varepsilon^{(0)}_{\alpha 3} &= \frac{1}{2}\Big(\varphi_\alpha + u_{3,\alpha} + b^\lambda_\alpha u_\lambda + a^{\lambda\gamma}u_{\lambda|\alpha}\varphi_\gamma - b^\lambda_\alpha\varphi_\lambda u_3 + \varphi_3 u_{3,\alpha} + b^\lambda_\alpha u_\lambda\varphi_3\Big) \\ \varepsilon^{(1)}_{\alpha 3} &= \frac{1}{2}\Big(\varphi_{3,\alpha} + a^{\lambda\gamma}\varphi_{\lambda|\alpha}\varphi_\gamma + \varphi_3\varphi_{3,\alpha} + 2\psi_3 u_{3,\alpha} + 2\psi_3 b^\lambda_\alpha u_\lambda\Big) \\ \varepsilon^{(0)}_{33} &= \frac{1}{2}\Big(2\varphi_3 + a^{\lambda\gamma}\varphi_\lambda\varphi_\gamma + (\varphi_3)^2\Big) \\ \varepsilon^{(1)}_{33} &= 2\left(\psi_3 + \varphi_3\psi_3\right) \end{aligned} \tag{9}$$

where $c_{\alpha\beta} = b_{\alpha\mu}b^\mu_\beta$ is the covariant third fundamental form of the reference surface. Note that the component $\varepsilon^{(1)}_{33}$ vanishes when $\psi_3 = 0$ (6-parameter formulation).

The second Piola-Kirchhoff stress tensor is used for the Lagrangian formulation and is energetically-conjugate to the rate of Green strain tensor $\dot{\mathbf{E}}$ (Reddy, 2004). Like $\mathbf{E}$, the second Piola-Kirchhoff stress tensor $\mathbf{S}$ is transformed to the midsurface M_R by

$$\hat{\mathbf{S}} = \boldsymbol{\mu}^{-1}\mathbf{S}\,\boldsymbol{\mu}^{-T} = \Phi^*\left(\mathbf{S}\right) \tag{10}$$

which is the pull-back operator of the contravariant tensor $\mathbf{S}$.

Let $\mathbf{M}^n$ denote the *stress resultant tensor* which is a symmetric tensor. The tensor $\mathbf{M}^n$ is defined as

$$\left[\mathbf{M}^0, \mathbf{M}^1\right] = \int_{-h/2}^{h/2} \left[1, \theta^3\right] \hat{\mathbf{S}} \mu \, d\theta^3 \tag{11}$$

The scalar quantity μ is the determinant of the shifter tensor $\boldsymbol{\mu}$. The stress resultant tensors are also energetically-conjugate to the strain resultants $\boldsymbol{\varepsilon}^i$. The stress resultant tensors may be decomposed in component form as

$$\begin{aligned} \mathbf{M}^0 &= \overset{(0)}{N}{}^{\alpha\beta} \, \mathbf{a}_\alpha \otimes \mathbf{a}_\beta + \overset{(0)}{Q}{}^{\alpha 3} (\mathbf{a}_\alpha \otimes \mathbf{a}_3 + \mathbf{a}_3 \otimes \mathbf{a}_\alpha) + \overset{(0)}{T}{}^{33} \, \mathbf{a}_3 \otimes \mathbf{a}_3 \\ \mathbf{M}^1 &= \overset{(1)}{N}{}^{\alpha\beta} \, \mathbf{a}_\alpha \otimes \mathbf{a}_\beta + \overset{(1)}{Q}{}^{\alpha 3} (\mathbf{a}_\alpha \otimes \mathbf{a}_3 + \mathbf{a}_3 \otimes \mathbf{a}_\alpha) + \overset{(1)}{T}{}^{33} \, \mathbf{a}_3 \otimes \mathbf{a}_3 \end{aligned} \tag{12}$$

where $\overset{(n)}{N}{}^{\alpha\beta}$, $\overset{(n)}{Q}{}^{\alpha 3}$ and $\overset{(n)}{T}{}^{33}$ are membrane, shear and stretching components, respectively.

1.3. Functionally Graded Shells

In this section we consider a hyperelastic and inhomogeneous shell. The shell structure can undergo large deformations (rotations and displacements) while the material response remains in the elastic regime. We also consider the relation between the second Piola-Kirchhoff stress tensor $\mathbf{S}$ and the Green strain tensor $\mathbf{E}$ is linear. It implies that

$$\mathbf{S} = \mathbb{C} \cdot \mathbf{E} \tag{13}$$

where $\mathbb{C}$ is the fourth-order elasticity tensor. The tensor $\mathbb{C}$ is represented in convected coordinates as

$$\mathbb{C} = C^{ijkl} \, \mathbf{g}_i \otimes \mathbf{g}_j \otimes \mathbf{g}_k \otimes \mathbf{g}_l \tag{14}$$

where the components of $\mathbb{C}$ satisfy the following symmetry conditions

$$C^{ijkl} = C^{jikl} = C^{ijlk} = C^{klij} \tag{15}$$

Functionally graded materials (FGMs) are a special kind of composites in which the material properties vary smoothly and continuously from one surface to the other. These materials are microscopically inhomogeneous and are typically made from isotropic components. One of the main advantages of FGMs is that it mitigates severe stress concentrations and singularities at intersections between interfaces usually presented in laminate composites due to their abrupt transitions in material compositions and properties. Applications of FGMs are extensive especially in high-temperature environments such as nuclear reactors, chemical plants and high-speed spacecrafts.

The materials in the bottom and top surfaces are usually metal and ceramic respectively (Fig. 2). Material properties at a point $\mathbf{X}$ are given by a combination between metal and ceramic constituents, i.e. by the weighted average of the moduli of the constituents, namely

$$\varpi\left(\theta^3\right) = \varpi_c f_c + \varpi_m f_m \tag{16}$$

where the subscripts *m* and *c* refer to the metal and ceramic constituents and *f* is the volume

fraction of the phase. The symbol ϖ denotes a generic material property.

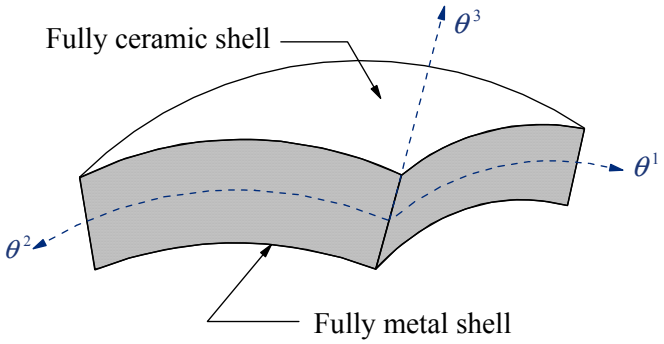

Fig. 2. Functionally graded shell.

The volume fractions of the ceramic f_c and metal f_m corresponding to the power law are expressed as (Reddy, 2000; Praveen and Reddy, 1998; Reddy and Chin, 1998)

$$f_c = \left(\frac{z}{h} + \frac{1}{2}\right)^n, \quad f_m = 1 - f_c \tag{17}$$

where n is the volume fraction exponent which takes values greater than or equal to zero. The value of n equal to zero represents a fully ceramic shell. Conversely, we have a fully metal shell as n tends to infinity (Fig. 3).

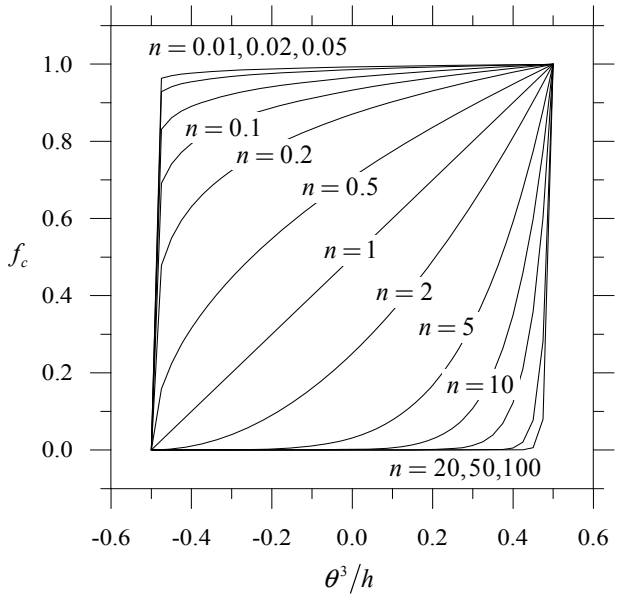

Fig. 3. Variation of the volume fraction function f_c through the dimensionless thickness for different values of power-law index n.

The components of the elasticity tensor $C^{ijkl}\left(\theta^3\right)$ are functions of the thickness coordinate. They can be written in terms of the convected base vectors as

$$\mathbb{C} = C^{ijkl}\left(\theta^3\right)\mathbf{g}_i \otimes \mathbf{g}_j \otimes \mathbf{g}_k \otimes \mathbf{g}_l \tag{18}$$

which can be arranged in a matrix $\left[C^{ijkl}\right] \in \mathbb{M}^{6\times 6}$ such that

$$\left[C^{ijkl}\right] = \begin{bmatrix} C^{1111} & C^{1122} & C^{1133} & 0 & 0 & 0 \\ C^{1122} & C^{2222} & C^{2233} & 0 & 0 & 0 \\ C^{1133} & C^{2233} & C^{3333} & 0 & 0 & 0 \\ 0 & 0 & 0 & C^{2323} & 0 & 0 \\ 0 & 0 & 0 & 0 & C^{1313} & 0 \\ 0 & 0 & 0 & 0 & 0 & C^{1212} \end{bmatrix}_{6\times 6} \tag{19}$$

The components C^{ijkl} at each θ^3 are functions of only two independent variables. then

$$\begin{aligned} C^{1111} = C^{2222} = C^{3333} &= \frac{E\left(\theta^3\right)(1-\nu)}{(1+\nu)(1-2\nu)} \\ C^{1122} = C^{1133} = C^{2233} &= \frac{E\left(\theta^3\right)\nu}{(1+\nu)(1-2\nu)} \\ C^{1212} = C^{1313} = C^{2323} &= \frac{E\left(\theta^3\right)}{2(1+\nu)} \end{aligned} \tag{20}$$

where $E\left(\theta^3\right) = E_c f_c + E_m f_m$. The Poisson's ratio ν is considered constant through the thickness. Hence

$$\begin{aligned} C^{ijkl}\left(\theta^3\right) &= C_c^{ijkl} f_c + C_m^{ijkl} f_m \\ &= C_{cm}^{ijkl} f_c + C_m^{ijkl} \end{aligned} \tag{21}$$

where $C_{cm}^{ijkl} = C_c^{ijkl} - C_m^{ijkl}$ and f_c, f_m are given in (17).

1.4. Weak Formulation

The finite element framework is based on the principle of virtual work. Our analysis is restricted to static cases. The virtual work statement is nothing but the weak form of the equilibrium equations and it is valid for linear and nonlinear stress-strain relations (Reddy, 2002).

The abstract configuration solution of the shell is denoted by the set

$$\mathsf{C} = \left\{ \Phi \equiv \left(\mathbf{u}, \boldsymbol{\varphi}, \underline{\boldsymbol{\psi}}\right) \middle| \Phi : \mathsf{A} \quad \in \mathbb{R}^2 \rightarrow \mathbb{R}^3 \times \mathbb{R}^3 \times \mathbb{R} \right\} \tag{22}$$

where A is the parametric space of the midsurface. Note that $\Phi \in \mathsf{C}$ contains the same amount of three-dimensional information as Eq. (2) to locate at any time arbitrary points in the three-dimensional shell.

We express the weak formulation as

$$\mathcal{G}(\Phi,\delta\Phi)=\mathcal{G}_{\text{int}}(\Phi,\delta\Phi)+\mathcal{G}_{\text{ext}}(\Phi,\delta\Phi)=0 \tag{23}$$

where

$$\mathcal{G}_{\text{int}}(\Phi,\delta\Phi)=\int_{\mathsf{M}_R}(\mathbf{M}^0\cdot\delta\boldsymbol{\varepsilon}^0+\mathbf{M}^1\cdot\delta\boldsymbol{\varepsilon}^1)\,d\Omega \tag{24}$$

$$\begin{aligned}\mathcal{G}_{\text{ext}}(\Phi,\delta\Phi)=&-\int_{\mathsf{M}_R}(\mathbf{p}\cdot\delta\mathbf{u}+\mathbf{l}\cdot\delta\boldsymbol{\varphi}+\mathbf{k}\cdot\delta\underline{\boldsymbol{\psi}})\,d\Omega\\&-\int_{\partial\mathsf{M}_R}(\mathbf{p}^s\cdot\delta\mathbf{u}+\mathbf{l}^s\cdot\delta\boldsymbol{\varphi}+\mathbf{k}^s\cdot\delta\underline{\boldsymbol{\psi}})\,ds\end{aligned} \tag{25}$$

For hyperelastic materials, the static part of the weak form of the equilibrium equations is the first variation of an elastic potential energy function. This statement is known as the principle of minimum total potential energy (Reddy, 2002). We define the elastic potential function $\Pi(\circ):\mathsf{C}\rightarrow\mathbb{R}$ as

$$\begin{aligned}\Pi(\Phi)=&\int_{\mathsf{B}_R}\rho_0\,\Psi\,dV-\int_{\mathsf{M}_R}(\mathbf{p}\cdot\mathbf{u}+\mathbf{l}\cdot\boldsymbol{\varphi}+\mathbf{k}\cdot\underline{\boldsymbol{\psi}})\,d\Omega\\&-\int_{\partial\mathsf{M}_R}(\mathbf{p}^s\cdot\mathbf{u}+\mathbf{l}^s\cdot\boldsymbol{\varphi}+\mathbf{k}^s\cdot\underline{\boldsymbol{\psi}})\,ds\end{aligned} \tag{26}$$

The first variation of the potential energy is given by

$$\mathcal{G}(\Phi,\delta\Phi)=\delta\Pi(\Phi,\delta\Phi)=D\Pi(\Phi)[\delta\Phi]=0 \tag{27}$$

To solve the nonlinear equations is to use the incremental/iterative method of Newton-Raphson. This procedure requires a linearization of the weak form generating recurrence update formulas. The linearization process relies on the concept of directional derivatives (Hughes and Pister, 1978; Bonet and Wood, 1997). We assume that the external forces are conservative (independent of Φ). Applying that procedure to equation (23) we obtain

$$\mathcal{LG}(\Phi,\delta\Phi;\Delta\Phi)=\mathcal{G}(\Phi,\delta\Phi)\underline{+D\mathcal{G}(\Phi,\delta\Phi)[\Delta\Phi]}+o(\Delta\Phi) \tag{28}$$

where the underlined term is called consistent tangent operator. Furthermore, we can write the tangent operator as

$$D\mathcal{G}(\Phi,\delta\Phi)[\Delta\Phi]=\nabla\mathcal{G}(\Phi,\delta\Phi)\cdot\Delta\Phi \tag{29}$$

since $\delta\Phi$ remains constant during the increment $\Delta\Phi$.

The iterative solution procedure goes as follows: given a configuration $\Phi^k\in\mathsf{C}$, corresponding to iteration *k*, solve the linearized system

$$\mathcal{G}(\Phi^k,\delta\Phi)+\nabla\mathcal{G}(\Phi^k,\delta\Phi)\cdot\Delta\Phi^k=0 \tag{30}$$

where $\Delta\Phi^k$ is the incremental change in the configuration of the shell. This increment is used to update the shell configuration $\Phi^k\rightarrow\Phi^{k+1}\in\mathsf{C}$. Namely

$$\Phi^{k+1}=\Phi^k+\Delta\Phi^k \tag{31}$$

Notice that the use of the triple $\left(\mathbf{u},\boldsymbol{\varphi},\underline{\boldsymbol{\psi}}\right)$ preserves the additive structure of the configuration update of the shell.

The consistent tangent operator is decomposed in two parts: the material tangent operator and the geometric tangent operator. Thus

$$D\mathcal{G}\left(\Phi,\delta\Phi\right)\left[\Delta\Phi\right]=D_m\mathcal{G}\left(\Phi,\delta\Phi\right)\left[\Delta\Phi\right]+D_g\mathcal{G}\left(\Phi,\delta\Phi\right)\left[\Delta\Phi\right] \tag{32}$$

The contribution of the external forces vanishes because they are conservative. The first term which is the material part is given by

$$D_m\mathcal{G}\left(\Phi,\delta\Phi\right)\left[\Delta\Phi\right]=\int_{\mathsf{M}_R}\sum_{n=0}^{1}(D\mathbf{M}^n\left[\Delta\Phi\right]\cdot\delta\boldsymbol{\varepsilon}^n)\,d\Omega \tag{33}$$

and the geometric part by

$$D_g\mathcal{G}\left(\Phi,\delta\Phi\right)\left[\Delta\Phi\right]=\int_{\mathsf{M}_R}\sum_{n=0}^{1}(\mathbf{M}^n\cdot D\delta\boldsymbol{\varepsilon}^n\left[\Delta\Phi\right])\,d\Omega \tag{34}$$

The material part of the tangent operator results from the directional derivative of the stress resultants. After some manipulations we obtain

$$D\mathbf{M}^i\left(\Phi\right)\left[\Delta\Phi\right]=\sum_{j=0}^{1}\int_{-h/2}^{h/2}\mu(\theta^3)^{i+j}\,\hat{\mathbb{C}}\cdot\Delta\boldsymbol{\varepsilon}^j\,d\theta^3 \tag{35}$$

where $\hat{\mathbb{C}}$ is the pull-back of the contravariant fourth-order elasticity tensor $\mathbb{C}$. Substituting (35) into (33) we arrive to

$$D_m\mathcal{G}\left(\Phi,\delta\Phi\right)\left[\Delta\Phi\right]=\int_{\mathsf{M}_R}\sum_{i=0}^{1}\sum_{j=0}^{1}(\delta\boldsymbol{\varepsilon}^i\cdot\mathbb{B}^{(i+j)}\cdot\Delta\boldsymbol{\varepsilon}^j)\,d\Omega, \tag{36}$$

where $\Delta\boldsymbol{\varepsilon}^j$ is can be easily calculated. The components of the fourth-order tensor $\mathbb{B}^{(k)}$ are the material stiffness coefficients of the shell and are defined as

$$\mathbb{B}^{(k)}=\int_{-h/2}^{h/2}\mu(\theta^3)^k\,\hat{\mathbb{C}}\,d\theta^3,\qquad k=0,1,2 \tag{37}$$

and are computed by Gauss integration.

The computation of virtual internal energy $\mathcal{G}_{\text{int}}$ and the tangent operator is not a trivial task. Even for isotropic materials these expressions have an extremely complex form when displacements and rotations are large.

Next, the finite element equations are obtained by interpolating the covariant components of the kinematic variables in terms of the base vectors $\mathbf{a}^\alpha$. Namely

$$\begin{gathered}\mathbf{u}^{hp}\left(\underline{\boldsymbol{\theta}}\right)=\left(\sum_{j=1}^{m}u_i^{(j)}N^{(j)}\left(\xi,\eta\right)\right)\mathbf{a}^i,\qquad\boldsymbol{\varphi}^{hp}\left(\underline{\boldsymbol{\theta}}\right)=\left(\sum_{j=1}^{m}\varphi_i^{(j)}N^{(j)}\left(\xi,\eta\right)\right)\mathbf{a}^i\\ \underline{\boldsymbol{\psi}}^{hp}\left(\underline{\boldsymbol{\theta}}\right)=\left(\sum_{j=1}^{m}\psi_3^{(j)}N^{(j)}\left(\xi,\eta\right)\right)\mathbf{a}^3\end{gathered} \tag{38}$$

where $\left(u_i^{(j)}, \varphi_i^{(j)}, \psi_3^{(j)}\right)$ denote the nodal values of the kinematic variables.

We then arrive to a system of highly nonlinear algebraic equations which can be written in matrix form by means of the stiffness and tangent matrices. The solution is carried out by subroutines written in FORTRAN.

1.5. Numerical Examples

In this section, numerical results obtained by the model developed herein are presented for shell structures. Typical benchmark problems for isotropic and homogeneous shells are investigated for bending behavior of their counterparts functionally graded shells.

Regular meshes of $Q25$, $Q49$ and $Q81$ high-order elements with seven degrees of freedom per node were utilized in the finite element analysis (see Table 1). By increasing the p level or refining the finite element mesh, we mitigate locking problems. Full Gauss integration rule is employed in all examples.

Table 1. Number of degrees of freedom per element for different p levels

Element	p level	FSDT (DOF)
Q4	1	28
Q9	2	63
Q25	4	175
Q49	6	343
Q81	8	567

Roll-up of a functionally graded plate strip

We consider a FGM plate strip subjected to a bending distributed moment on the other end (Fig. 4). The isotropic and homogeneous counterpart has been considered Simo et al. (1990) as well as Betsch et al. (1998). This problem is good to test the capability of the finite element model to simulate large rotations on shells.

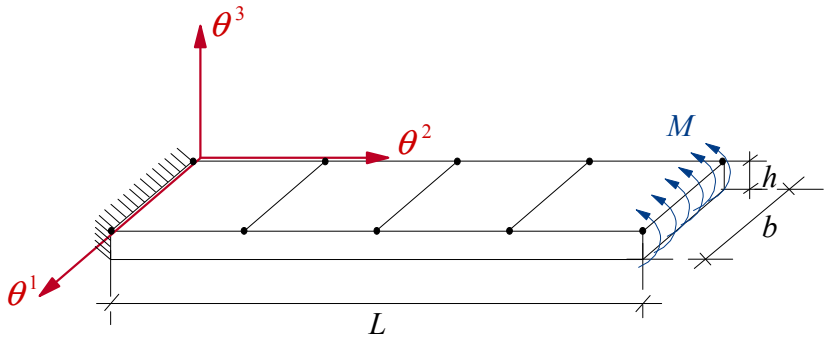

Fig. 4. Cantilever FGM plate strip under end bending moment.

The material properties and geometry of the plate are

$$E_m = 0.7\times10^9, \quad E_c = 1.51\times10^9, \quad \nu = 0.3$$
$$L = 12.0, \quad b = 1.0, \quad h = 0.1$$
$$M_{\text{REF}} = 65886.17926$$

Figures 5 and 6 depict tip displacements of the cantilever strip plate versus the end bending moment for various volume fraction exponents n (from fully ceramic to fully metal). We utilize a regular mesh of $1\times8Q25$ elements for the finite element discretization. The Newton method exhibits a good rate of convergence until some displacement level and then it diverges (for inhomogeneous shell cases). It is not clear for the authors why this problem happens. It seems that for these cases we do not have real solutions. However, before arriving to any conclusion further studies are needed.

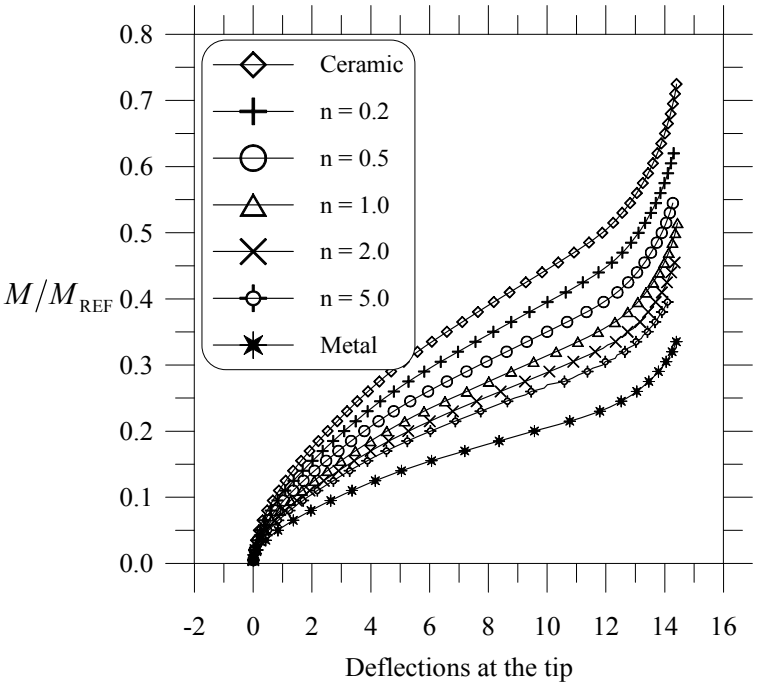

Fig. 5. Tip-deflection $-u_{<1>}$ vs. end moment M for the FGM plate strip.

Figure 7 shows the undeformed and deformed configuration of a FGM strip plate for various load stages and $n = 1.0$. The plate shows large rotations beyond 180° with deformed configurations similar to the homogeneous case.

Annular FGM plate under end shear force

We analyze an annular FGM plate subjected to a distributed transverse shear force (Fig. 8). This benchmark problem was considered for homogeneous and isotropic plates by Büchter and Ramm (1992) and Sansour and Kollmann (2000); and for multilayered composites by Arciniega and Reddy (2006). The material properties are the same as the last example and will be used in all examples. The geometric quantities are given by

$$R_i = 6,\ R_e = 10,\ h = 0.03$$

for a maximum distributed force of $q_{\max} = 20.0$.

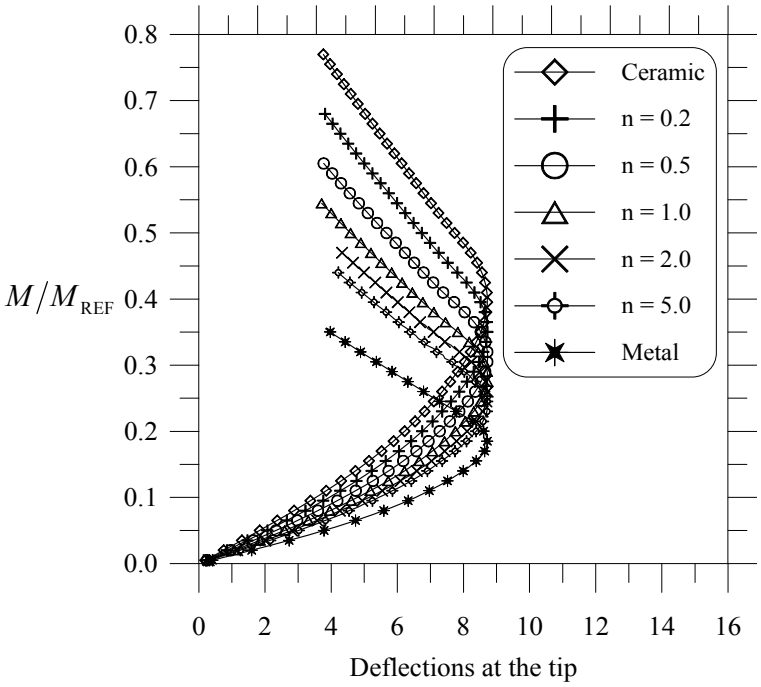

Fig. 6. Tip-deflection $u_{<3>}$ vs. end moment M for the FGM plate strip.

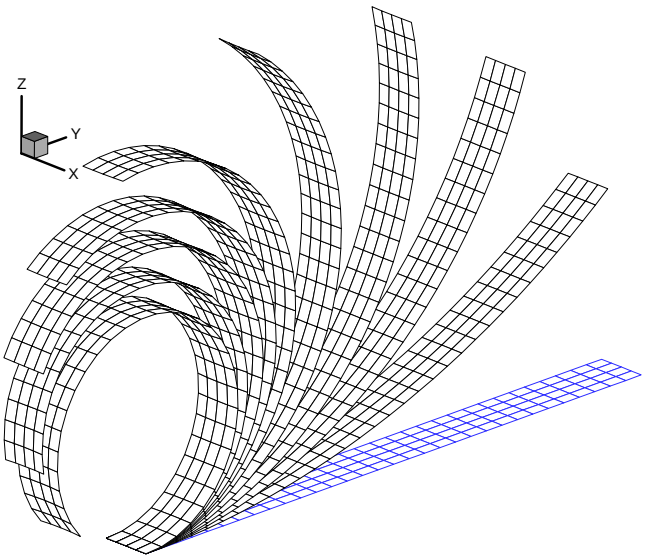

Fig. 7. Deformed configurations of a FGM plate (n = 1.0) under end bending moment (load values $M/M_{\text{REF}} = 0.075, 0.15, \ldots, 0.6, 0.625$).

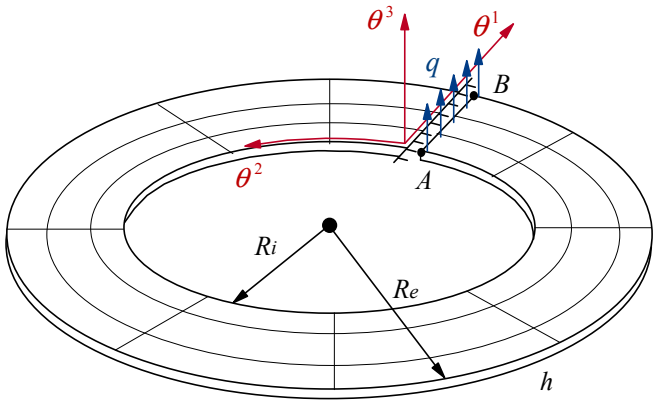

Fig. 8. Annular FGM plate strip under transverse end shear force.

The plate is modeled by polar coordinates. A regular mesh of $1\times5Q49$ elements (p level equal to 6) is used in the present analysis. Computation is performed by the Newton-Raphson method with 80 load steps and convergence tolerance for the residual forces of 1.0×10^{-4}.

The shear load versus displacement curves for two characteristic points are depicted in Figures 9 and 10. The deformed configurations of a FGM annular plate for various load levels and $n=2.0$ is shown in Fig. 11. It is clear that the plate undergoes large displacements at the corresponding loading of $F=80$.

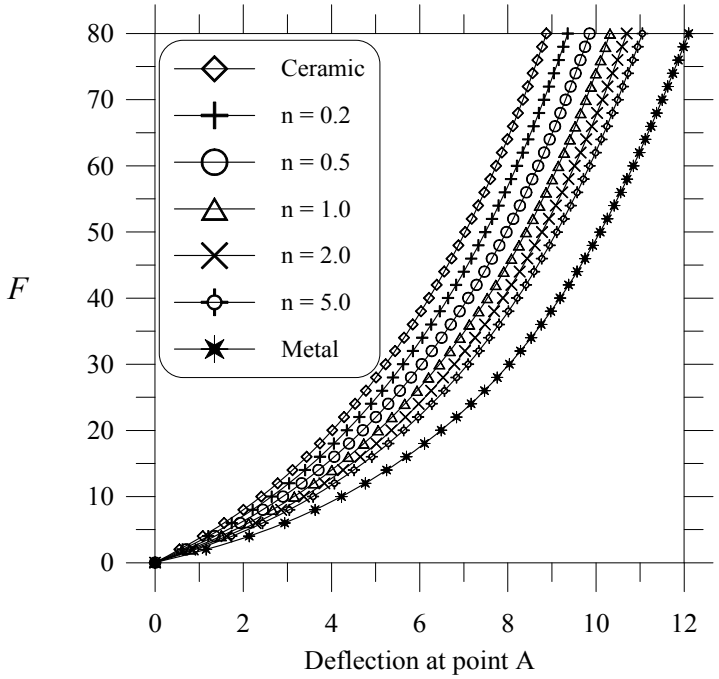

Fig. 9. Transverse displacement curves at point A vs. shear force $F=4q$ of the cantilever annular plate strip.

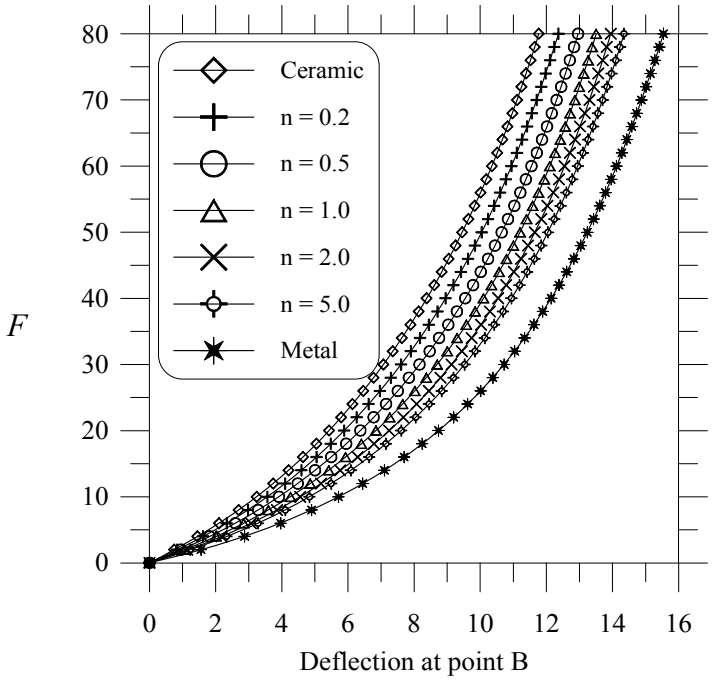

Fig. 10. Transverse displacement curves at point B vs. shear force $F = 4q$ of the cantilever annular plate strip.

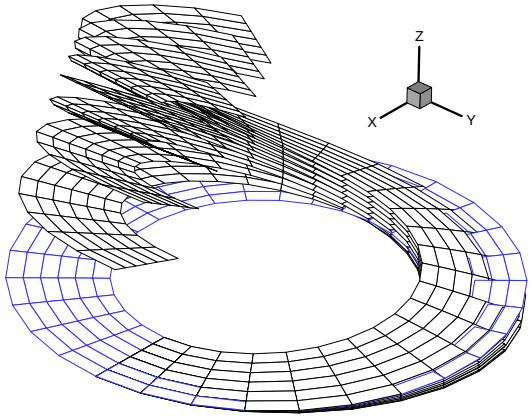

Fig. 11. Deformed configurations of a FGM plate strip (n = 2.0) under transverse end shear force (load values $F = 10, 20, \ldots, 80$).

Pull-out of a functionally graded cylindrical shell

The functionally graded cylindrical shell with free ends is subjected to two opposite loads (Fig. 12). The homogeneous case was considered by Brank et al. (1995) and Sansour and Kollmann (2000), among others. The following geometrical data is used in the analysis

$$L = 10.35,\ R = 4.953,\ h = 0.094$$

An octant of the shell is modeled using 2×2 $Q81$ elements which is enough to overcome locking problems. The Newton-Raphson method with 80 load steps is utilized with equal load steps of 60000. The adopted error tolerance for the residual was 1.0×10^{-5}.

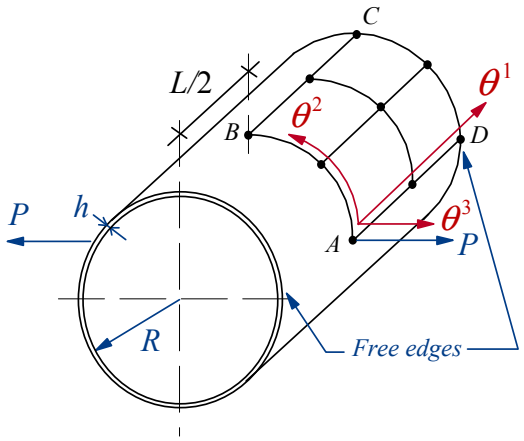

Fig. 12. Pull-out of a FGM cylinder with free edges.

Figures 13 to 15 show the radial displacements at points A, B and C of the shell, respectively. Convergence rates for this example are quite good (3 to 5 iterations per load step). As expected, bending response of FGM cylinders lies in between of the fully ceramic and fully metal shells. The deformed configurations for a FGM cylindrical shell is depicted in Fig. 16 for $P = 5.1\times10^{6}$ and $n = 1.0$.

FGM hemisphere under internal pressure

The last example considered is a cylindrical FGM shell under internal pressure (Fig. 17). This is not a following loading (independent of the displacements).The cylinder has fixed boundary conditions on both ends. The geometric data is as follows:

$$a = 20.0,\ R = 5.0,\ h = 0.01$$

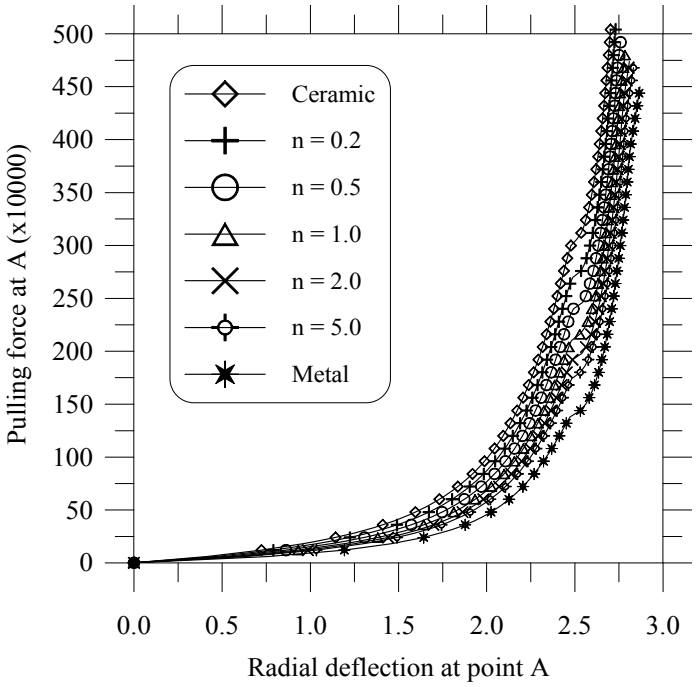

Fig. 13. Radial displacements at point A $(u_{<3>})$ vs. pulling force of a FGM cylinder with free edges.

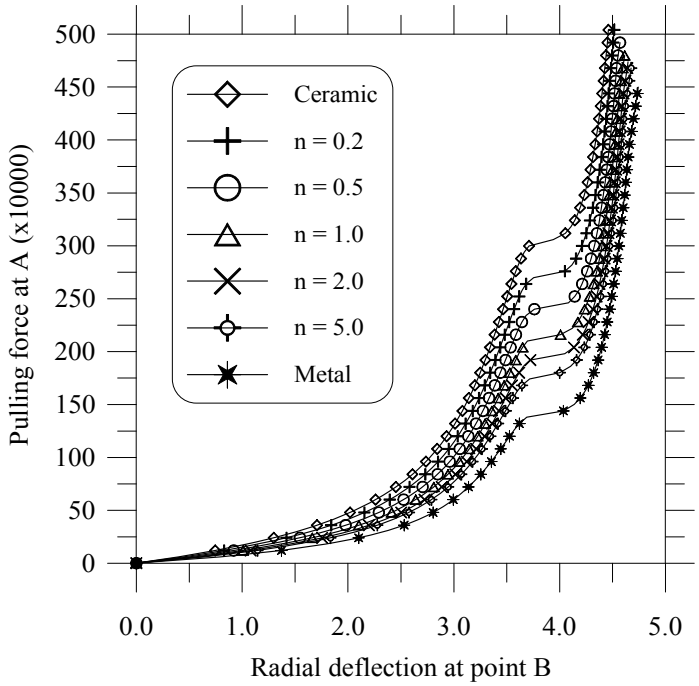

Fig. 14. Radial displacements at point B $(-u_{<3>})$ vs. pulling force of a FGM cylinder with free edges.

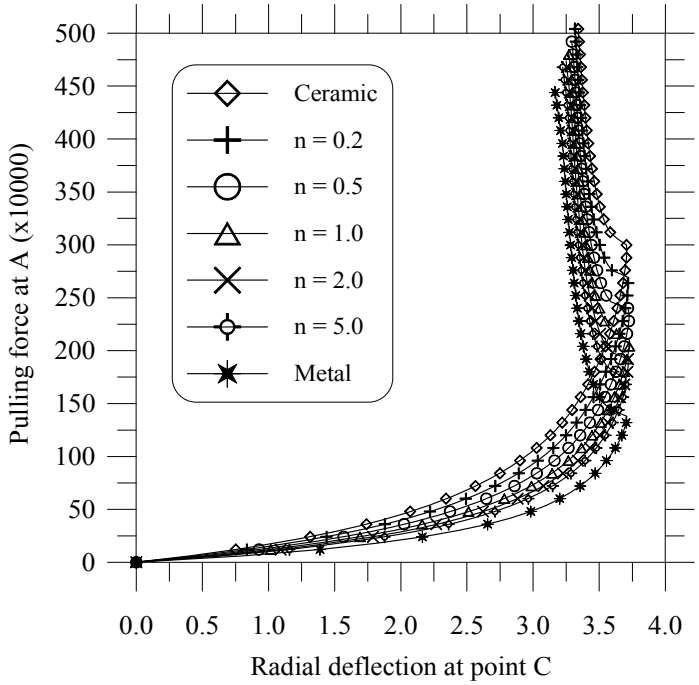

Fig. 15. Radial displacements at point C $(-u_{<3>})$ vs. pulling force of a FGM cylinder with free edges.

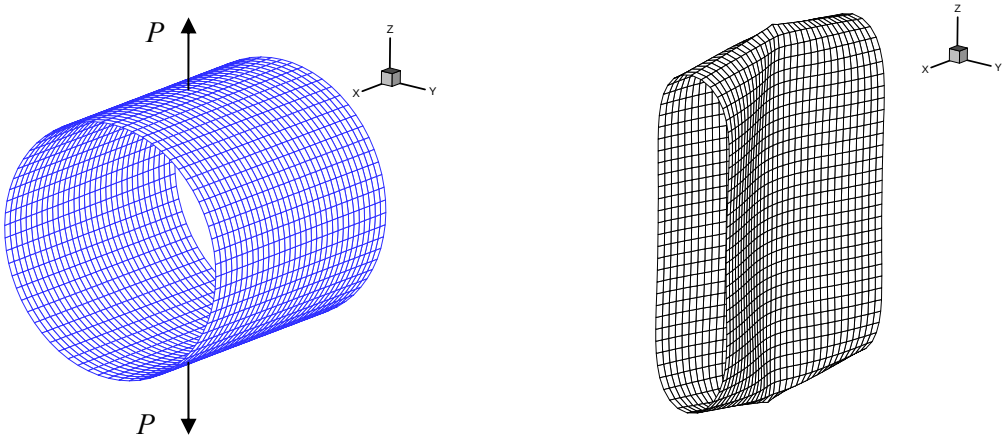

Fig. 16. Deformed configurations of the FGM cylinder under pulling forces. Load $P = 5.1\times10^{6}$ $(n = 1.0)$.

FGM hemisphere under internal pressure

The last example considered is a cylindrical FGM shell under internal pressure (Fig. 17). The cylinder has fixed boundary conditions on both ends. The geometric data is as follows: $a = 20.0, R = 5.0, h = 0.01$

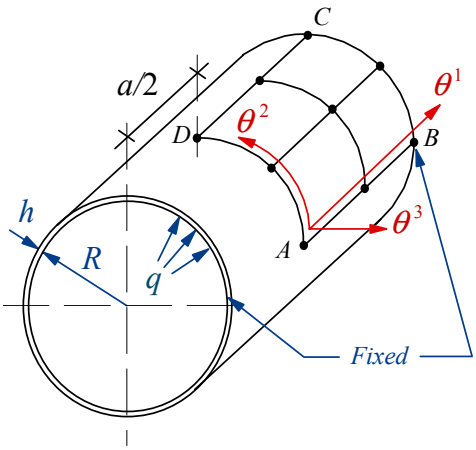

Fig. 17. FGM cylindrical shell under internal pressure.

A regular mesh of 2×2Q81 elements is used in the analysis. We take advantage of the symmetry of the shell and only an octant of the shell is considered as the computational domain. Figure 18 shows the radial deflections at the central point versus the internal pressure for FGM cylinders. We notice that FGM cylinders with low values of n exhibit stiffer response than those with high volume fraction exponent (more metal than ceramic). The final configuration of a FGM cylinder for $n = 5.0$ is depicted in Fig. 19.

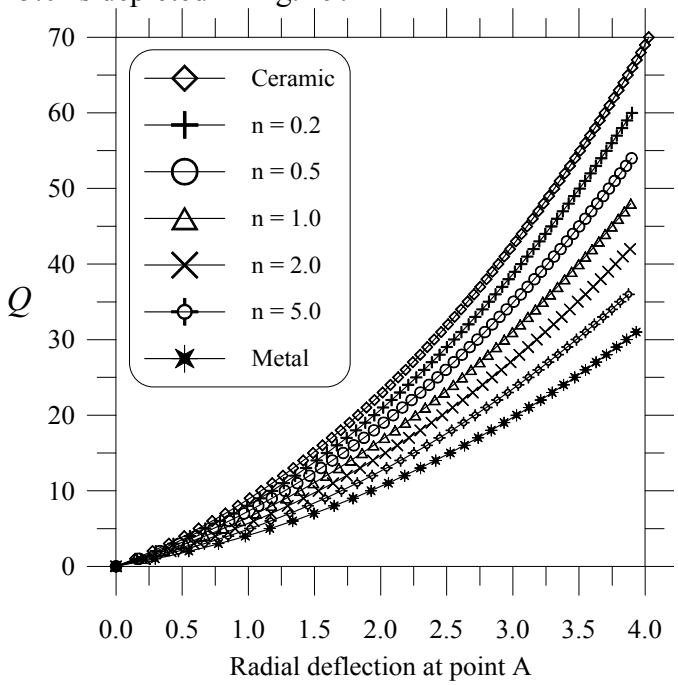

Fig. 18. Radial deflection at A vs. pressure load ($Q = 10^6 q$) of a FGM cylindrical shell.

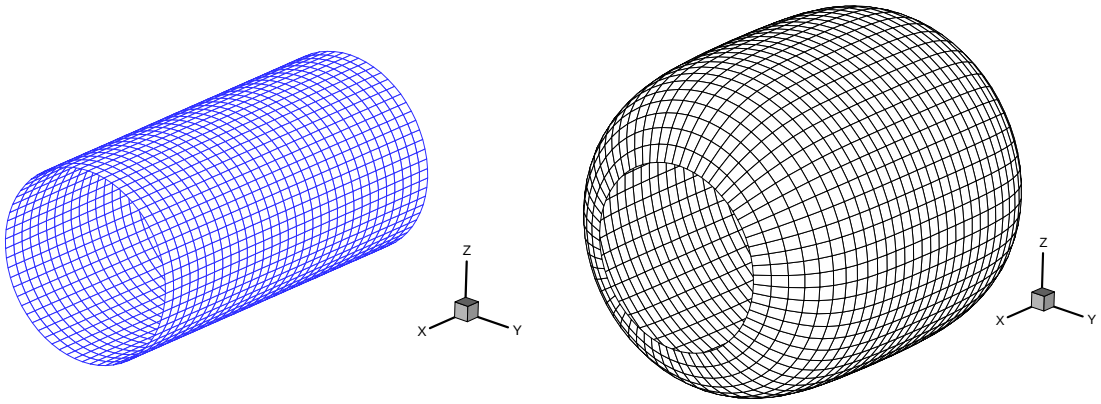

Fig. 19. Deformed configuration of a FGM cylindrical shell. Loading $q = 3.6\times10^{6}$ ($n = 5.0$).

1.6. Conclusions

In this paper we present a large deformation analysis for functionally graded shells. We consider a through-the-thickness variation of the material properties of the FGM shell which is made of two isotropic constituents. The gradation of properties through the thickness is assumed to be of the power law type. A tensor-based finite element model is developed for geometric nonlinear analysis of the shell. This approach showed to be reliable and efficient. The derived first-order shell theory with seven parameters with exact nonlinear deformations is consistent and simple. It incorporates thickness changes in the model, and then full 3D constitutive equations are utilized. A family of High-order Lagrangian elements was introduced to avoid membrane and shear locking for shells. We found that the nonlinear bending response of FGM shells under mechanical loading lies between that of ceramic and metal shells, as expected. The patterns of load-displacement equilibrium curves of FGM shells are similar to those of isotropic and homogeneous counterparts. Numerical examples for plates and cylindrical shells, presented herein, illustrate the validity of the present approach and the developed formulation for FGM shells.

1.7. References for Section 1

Arciniega, R.A., Reddy, J.N., 2005. Consistent third-order shell theory with application to composite circular cylinders. *AIAA J.* 43 (9), 2024-2038.

Arciniega, R.A., Reddy, J.N., 2006. Tensor-based finite element formulation for geometrically nonlinear analysis of shell structures. Comput. Methods Appl. Mech. Engrg.

Balah, M., Al-Ghamedy, H.N., 2002. Finite element formulation of a third-order laminated finite rotation shell element, *Comput. Struct*. 80, 1975-1990.

Başar, Y., Ding, Y., Schultz, R., 1993. Refined shear-deformation models for composite laminates with finite rotations. *Int. J. Solids Struct*. 30 (1993) 2611-2638.

Betsch, P., Menzel, A., Stein, E., 1998. On the parametrization of finite rotations in computational mechanics: A classification of concepts with application to smooth shells. *Comput. Methods Appl. Mech. Engrg*. 155, 273-305.

Bischoff, M., Ramm, E., 1997. Shear deformable shell elements for large strains and rotations. *Int. J. Numer. Meth. Engrg*. 40, 4427-4449.

Bonet, J., Wood, R.D., 1997. *Nonlinear Continuum Mechanics for Finite Element Analysis.* Cambridge University Press, Cambridge.

Brank, B., Perić, D., Damjanić, F.B., 1995. On implementation of a four node shell element for thin multilayered elastic shells. *Comput. Mech*. 16, 341-359.

Büchter, N., Ramm, E., 1992. Shell theory vs. degeneration - A comparison in large rotation finite element analysis. *Int. J. Numer. Meth. Engrg*. 34, 39-59.

Della Croce, L., Venini, P., 2004. Finite elements for functionally graded Reissner-Mindlin plates. *Comput. Methods Appl. Mech. Engrg*. 193, 705-725.

Green, A.E., Zerna, W., 1968. Theoretical Elasticity. Clarendon Press, 2nd edition, Oxford.

Habip, L.M., 1965. Theory of elastic shells in the reference state. *Arch. Appl. Mech*. 34, 228-237.

Harte, R., Eckstein, U., 1986. Derivation of geometrically nonlinear finite shell elements via tensor notation. *Int. J. Numer. Meth. Engrg*. 23, 367-384.

Hughes, T.J., Pister, K.S., 1978. Consistent linearization in mechanics of solids and structures. *Comput. Struct.* 8, 391-397.

Koizumi, M., 1997. FGM activities in Japan. *Compos. Part B: Engrg*. 28B, 1-4.

Ma, L.S., Wang, T.J., 2003. Nonlinear bending and postbuckling of functionally graded circular plates under mechanical and thermal loadings. *Int. J. Nonlinear Mech*. 40, 3311-3330.

Na, K.S., Kim, J.H., 2005. Nonlinear bending response of functionally graded plates under thermal loads. J. Thermal Stresses 29, 245-261.

Naghdi, P.M., 1963. Foundations of elastic shell theory. In: *Progress in Solid Mechanics*, Vol. 4. North-Holland, Amsterdam.

Naghdi, P.M., 1972. Theory of shells and plates. In: *Handbuch der Physik*, VIa/2, Springer-Verlag, Berlin.

Pietraszkiewicz, W., 1979. *Finite Rotations and Lagrangean Description in the Nonlinear Theory of Shells*. Polish Scientific Publishers, Warszawa.

Praveen, G.N., Reddy, J.N., 1998. Nonlinear transient thermoelastic analysis of functionally graded ceramic-metal plates. *Int. J. Solids Struct*. 35, 4457-4476.

Reddy, J.N., 2000. Analysis of functionally graded plates. *Int. J. Numer. Meth. Engrg*. 47, 663-684.

Reddy, J.N., 2002. *Energy Principles and Variational Methods in Applied Mechanics*, 2nd edition, JohnWiley & Sons Inc., New York.

Reddy, J.N., 2004. *Mechanics of Laminated Composite Plates and Shells: Theory and Analysis*. 2nd ed., CRC Press, Boca Raton, Florida.

Reddy, J.N., Chin, C.D., 1998. Thermomechanical analysis of functionally cylinders and plates. *J. Thermal Stresses* 21, 593-626.

Reddy, J.N., Arciniega, R.A., 2004. Shear deformation plate and shell theories: From Stavsky to present. *Mech. Advanced Mater. Struct*. 11, 535-582.

Reddy, J.N., Arciniega, R.A., 2006a. Mechanical and thermal buckling of functionally graded ceramic-metal plates. In: *Analysis and Design of Plated Structures: Stability*. Woodhead Publishing, Cambridge, UK.

Reddy, J.N., Arciniega, R.A., 2006b. Free Vibration Analysis of Functionally Graded Plates. In: *Analysis and Design of Plated Structures: Dynamics*. Woodhead Publishing, Cambridge, UK.

Sansour, C., 1995. A theory and finite element formulation of shells at finite deformations involving thickness change: Circumventing the use of a rotation tensor. *Arch. Appl. Mech.* 65, 194-216.

Sansour, C., Kollmann, F.G., 2000. Families of 4-nodes and 9-nodes finite elements for a finite deformation shell theory. An assessment of hybrid stress, hybrid strain and enhanced strain elements. *Comput. Mech*. 24, 435-447.

Simo, J.C., Fox, D.D., Rifai, M.S., 1990. On a stress resultant geometrically exact shell model. Part III: Computational aspects of the nonlinear theory. *Comput. Methods Appl. Mech. Engrg*. 79, 21-70.

Vu-Quoc, L., Tan, X.G., 2003. Optimal solid shells for nonlinear analyses of multilayered composites. I. Statics. *Comput. Methods Appl. Mech. Engrg*. 192, 975-1016.

Woo, J., Meguid, S.A., 2001. Nonlinear analysis of functionally graded plates and shallow shells. *Int. J. Solids Struct*. 38, 7409-7421.

Yamanouchi, M., Koizumi, M., Hirai, T., Shiota, I., 1990. *Proceeding for the First International Symposium of Functionally Graded Materials*. Japan.

Yang, J., Shen, H.S., 2003a. Nonlinear bending analysis of shear deformable functionally graded plates subjected to thermomechanical loads under various boundary conditions. *Compos. Part B: Engrg*. 34, 103-115.

Yang, J., Shen, H.S., 2003b. Nonlinear analysis of functionally graded plates under transverse and in-plane loads. *Int. J. Nonlinear Mech*. 38, 467-482.

2. MIXED LEAST-SQUARES FINITE ELEMENT MODELS FOR STATIC AND FREE VIBRATION ANALYSIS OF PLATES

2.1. Introduction

Finite element models for the analysis of multilayered composite plate and shell structures have been widely developed in the last few decades. In overview, the main approaches to establish plate and shell theories have been in the framework of the so called axiomatic theories. The formulations differ in equivalent single-layer or layerwise variable descriptions and also in the choice for the unknown variables, resulting in displacement, stress or mixed formulations [1-3]. Traditionally, variational principles have been established to derive governing equations consistent with the chosen formulations. The widespread displacement formulations usually relate to the well-known principle of virtual displacement and the alternative mixed formulations typically derive from the Hu-Washizu or the Hellinger-Reissner variational principles [4,5].
Naturally, classical finite element models that were originally developed for one-layered isotropic structures were extended in a straightforward manner to multilayered plates and shells [6,7]. The classical lamination theory (CLT), first-order shear deformation theory (FSDT) and high-order theories have been known to provide a sufficiently accurate description of the global response of multilayered structures, as long as thin to moderately thick. Understandably, for a detailed response of individual layers or local phenomena description one must use layerwise theories (LWT) or the so called zig-zag theories that were indeed entirely originated and devoted to layered structures. In fact, one crucial issue for these theories is the fulfilment of the C_z^0-requirements. Basically, this means that displacements and transverse stresses must be C^0-continuous functions in the thickness direction due to interlaminar compatibility and equilibrium reasons.

The motivation for the proposed finite element models comes from earlier works on mixed finite element formulations based on least-squares variational principle. Namely, works by Pontaza and Reddy [8], Pontaza [9] and also, Duan and Lin [10]. Overall, the least-squares finite element formulations have shown promising theoretical and computational advantages, both in fluid and in solid mechanics. Specifically, Pontaza and Reddy [8] developed a mixed model based on least-squares formulation for the bending of single-layered isotropic plates, using the classical plate theory and first-order shear deformation theory. The prospect of extending this model gave rise to the proposed mixed least-squares FSDT model for static analysis of laminated composite plates. Then, a pioneer attempt to use least-squares formulation in modal analysis led to the development of the mixed least-squares FSDT finite element model for free vibration analysis of laminated composite plates.

The least-squares formulations as any weighted residual formulation provide an alternative approach to the weak form finite element models, both displacement-based and mixed. In the framework of FSDT weak form models, displacement formulations are known to encounter computational difficulties when modelling thin plates. The finite elements become excessively stiff, which results in an erroneous underprediction of displacements in static analysis or else in a severe overprediction of frequencies in free vibration analysis. This phenomenon is known as shear-locking. In essence, it is due to the inability of shear deformable elements to accurately model bending within an element under a state of zero transverse shearing strain. Higher-order elements experience relatively less locking, but sometimes at the expense of

a slower convergence. Usually shear-locking problems are only avoided by numerical integration techniques. Another possibility is mixed formulations, where in addition to generalized displacements the stress resultants are also used as independent variables [11,12]. Mixed finite element models based on weak formulations need however, that the finite element approximation spaces satisfy a so called Inf-Sup condition, in order to be consistent models [13]. This fulfilment is in general known to be rather difficult to prove analytically. Furthermore, mixed weak form models yield symmetric but not positive-definite stiffness matrices, adding numerical complexity to the models. Alternatively, within weighted residual formulations, least-squares finite element models are distinctive for being solely based on the idea of minimizing the error introduced in the approximation of the governing equations. Then, the benefit of using least-squares variational principle along with mixed formulations is that it leads to a variational unconstrained minimization problem, where the finite element approximation spaces can be chosen independently. Therefore, stability requirements such as the Inf-Sup condition never arise. This is precisely the theoretical merit of mixed least-squares formulations as it was demonstrated in the aforementioned works on this matter [8-10].

The proposed mixed least-squares finite element models consider the FSDT with generalized displacements and stress resultants as independent variables, using equal-order interpolation, for either static or free vibration analysis of laminated composite plates. Specifically, high-order C^0 basis functions and full integration are used to develop the discrete finite element models, since it was established to be the appropriate way to truly minimize the least-squares functional. In fact, Pontaza and Reddy [8] and later Pontaza [9] demonstrated the exponential decay of the least-squares functional with increasing order of the element. Furthermore, the mixed least-squares model for static analysis uses the classical C^0 Lagrange basis functions, whereas the model for free vibration analysis developed later uses instead C^0 interpolant polynomials of Gauss-Lobatto-Legendre quadrature points, which are more suitable basis functions for high-order elements [14]. Both mixed least-squares discrete models, once the boundary conditions are properly imposed, yield a symmetric and positive-definite stiffness matrix. This is another benefit of mixed least-squares models as opposed to mixed weak form models, which is computationally preferable. Most interestingly, the pioneer mixed least-squares model for free vibration analysis yields a quadratic eigenvalue problem with symmetric matrices, which is rather atypical within conservative systems. Ultimately, both proposed models exhibit excellent predictive capabilities in the framework of the FSDT as demonstrated by numerical examples presented hereafter. In particular, it is also shown that both least-squares models based on high-order basis functions are insensitive to shear-locking.

This report is outlined as follows. It starts by introducing the governing equations consistent with the mixed FSDT finite element models for both static and free vibration analysis of laminated composite plates. Then, the proposed models are derived from the least-squares formulation and related finite element specifics are addressed. Selected numerical examples are presented to assess the predictive capabilities of the mixed least-squares models through static and free vibration analysis of four laminated composite plates with different boundary conditions and various side-to-thickness ratios. Lastly, the overall conclusions are discussed.

2.2 Governing Equations

Consider a laminated composite plate of total thickness h and composed of N orthotropic layers, as shown in Fig. 1. Typically, the layers are unidirectional fibre-reinforced laminas whose in-

plane material coordinate axes are parallel and transverse to the fibres direction. Thus, the orientation of the *k*th layer is defined by an angle θ_k between the plate coordinate *x* and the fibres direction. In the *xy*-plane, $\overline{\Omega}$ represents the undeformed midplane of the plate and Ω the open bounded region with the boundary $\Gamma = \partial\Omega$. The *z*-axis is taken positive upward from the midplane. Specifically, the *k*th layer is located between the interfaces $z = z_k$ and $z = z_{k+1}$ in the thickness direction.

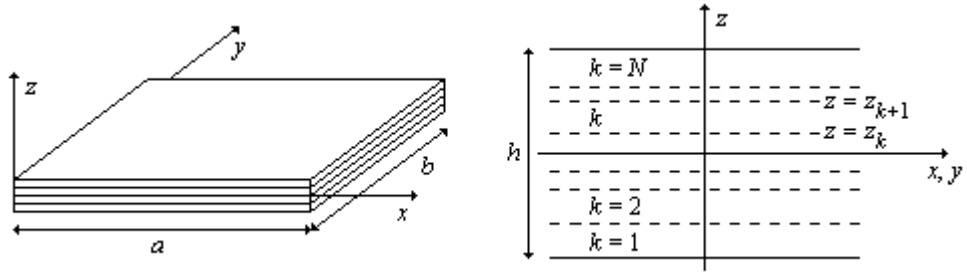

Figure 1. Notations for a laminated composite plate.

As previously mentioned, the adopted mixed formulation uses the generalized displacements and stress resultants as independent variables. Accordingly, for static analysis of laminated composite plates under a transverse load $q(x,y)$, the governing equations by the FSDT are the following (see Reddy [7]):

$$\underline{\partial}_{\varepsilon}^{\mathrm{T}}\mathbf{N} = 0 \qquad \text{in } \Omega \qquad (1)$$

$$\nabla\cdot\mathbf{Q} + q = 0 \qquad \text{in } \Omega \qquad (2)$$

$$\underline{\partial}_{\varepsilon}^{\mathrm{T}}\mathbf{M} - \mathbf{Q} = 0 \qquad \text{in } \Omega \qquad (3)$$

$$\mathbf{N} - \underline{\mathbf{A}}\,\underline{\partial}_{\varepsilon}\mathbf{u} - \underline{\mathbf{B}}\,\underline{\partial}_{\varepsilon}\boldsymbol{\Phi} = 0 \qquad \text{in } \Omega \qquad (4)$$

$$\mathbf{M} - \underline{\mathbf{B}}\,\underline{\partial}_{\varepsilon}\mathbf{u} - \underline{\mathbf{D}}\,\underline{\partial}_{\varepsilon}\boldsymbol{\Phi} = 0 \qquad \text{in } \Omega \qquad (5)$$

$$\mathbf{Q} - \hat{\underline{\mathbf{A}}}\left(\nabla w + \boldsymbol{\Phi}\right) = 0 \qquad \text{in } \Omega \qquad (6)$$

For free vibration analysis, the loads are set to zero and the variables assume a periodic solution in time, with a frequency ω. Hence, the governing equations by the FSDT for free vibration analysis of laminated composite plates are in turn, as follows (see Reddy [7]):

$$\underline{\partial}_{\varepsilon}^{\mathrm{T}}\mathbf{N} + \omega^2 I_0\mathbf{u} + \omega^2 I_1\boldsymbol{\Phi} = 0 \qquad \text{in } \Omega \qquad (7)$$

$$\nabla\cdot\mathbf{Q} + \omega^2 I_0 w = 0 \qquad \text{in } \Omega \qquad (8)$$

$$\underline{\partial}_{\varepsilon}^{\mathrm{T}}\mathbf{M} - \mathbf{Q} + \omega^2 I_1\mathbf{u} + \omega^2 I_2\boldsymbol{\Phi} = 0 \qquad \text{in } \Omega \qquad (9)$$

$$\mathbf{N} - \underline{\mathbf{A}}\,\underline{\partial}_{\varepsilon}\mathbf{u} - \underline{\mathbf{B}}\,\underline{\partial}_{\varepsilon}\boldsymbol{\Phi} = 0 \qquad \text{in } \Omega \qquad (10)$$

$$\mathbf{M} - \underline{\mathbf{B}}\,\underline{\partial}_{\varepsilon}\mathbf{u} - \underline{\mathbf{D}}\,\underline{\partial}_{\varepsilon}\boldsymbol{\Phi} = 0 \qquad \text{in } \Omega \qquad (11)$$

$$\mathbf{Q} - \hat{\underline{\mathbf{A}}}\left(\nabla w + \boldsymbol{\Phi}\right) = 0 \qquad \text{in } \Omega \qquad (12)$$

For convenience, a compact notation is applied here which proves to be rather useful to develop the least-squares functional afterwards. Overall, for static analysis the governing equations

include the plate equilibrium equations in Eqs. (1)-(3) and the laminate linear constitutive equations in Eqs. (4)-(6), while for free vibration analysis the governing equations include the plate equations of periodic motion in Eqs. (7)-(9) and the same laminate constitutive equations repeated in Eqs. (10)-(12), all written in terms of the independent variables. Specifically, in the current notation, the in-plane displacements **u**, the transverse deflection *w*, the rotations **Φ**, the in-plane force resultants **N**, the moment resultants **M** and the transverse force resultants **Q**, are assumed to be in the form specified below:

$$\mathbf{u} = \begin{bmatrix} u_0 & v_0 \end{bmatrix}^{\mathrm{T}},\ \mathbf{N} = \begin{bmatrix} N_{xx} & N_{yy} & N_{xy} \end{bmatrix}^{\mathrm{T}} \tag{13a}$$

$$w = w_0,\ \mathbf{M} = \begin{bmatrix} M_{xx} & M_{yy} & M_{xy} \end{bmatrix}^{\mathrm{T}} \tag{13b}$$

$$\mathbf{\Phi} = \begin{bmatrix} \phi_x & \phi_y \end{bmatrix}^{\mathrm{T}},\ \mathbf{Q} = \begin{bmatrix} Q_x & Q_y \end{bmatrix}^{\mathrm{T}} \tag{13c}$$

In addition, the form of the differential operator used repeatedly in the previous governing equations is given by:

$$\underline{\partial}_{\varepsilon}^{\mathrm{T}} = \begin{bmatrix} \partial/\partial x & 0 & \partial/\partial y \\ 0 & \partial/\partial y & \partial/\partial x \end{bmatrix} \tag{14}$$

In the laminate constitutive equations, equally written in Eqs. (4)-(6) and in Eqs. (10)-(12), a matrix form for the laminate stiffnesses is considered as follows:

$$\underline{\mathbf{A}} = \begin{bmatrix} A_{11} & A_{12} & A_{16} \\ A_{12} & A_{22} & A_{26} \\ A_{16} & A_{26} & A_{66} \end{bmatrix},\ \underline{\hat{\mathbf{A}}} = K \begin{bmatrix} A_{55} & A_{45} \\ A_{45} & A_{44} \end{bmatrix} \tag{15a}$$

$$\underline{\mathbf{B}} = \begin{bmatrix} B_{11} & B_{12} & B_{16} \\ B_{12} & B_{22} & B_{26} \\ B_{16} & B_{26} & B_{66} \end{bmatrix},\ \underline{\mathbf{D}} = \begin{bmatrix} D_{11} & D_{12} & D_{16} \\ D_{12} & D_{22} & D_{26} \\ D_{16} & D_{26} & D_{66} \end{bmatrix} \tag{15b}$$

Here, A_{ij} are called the extensional stiffnesses, D_{ij} the bending stiffnesses and B_{ij} the bending-extensional coupling stiffnesses. The factor K represents the shear correction coefficient, which takes the standard value 5/6 in the later numerical examples. Specifically, the laminate stiffnesses A_{ij}, B_{ij} and D_{ij} are in turn defined in terms of the lamina stiffnesses, *i.e*. the lamina plane-stress reduced stiffnesses transformed to the *xy*-plane of the laminate, as shown (see Reddy [7]):

$$A_{ij} = \sum_{k=1}^{N} \overline{Q}_{ij}^{(k)} \left(z_{k+1} - z_k \right) \tag{16a}$$

$$B_{ij} = \frac{1}{2} \sum_{k=1}^{N} \overline{Q}_{ij}^{(k)} \left(z_{k+1}^2 - z_k^2 \right) \tag{16b}$$

$$D_{ij} = \frac{1}{3} \sum_{k=1}^{N} \overline{Q}_{ij}^{(k)} \left(z_{k+1}^3 - z_k^3 \right) \tag{16c}$$

Furthermore, the mass moments of inertia I_i introduced in the plate equations of periodic motion in Eqs. (7)-(9) are defined in terms of the laminas density, as also shown:

$$I_0 = \sum_{k=1}^{N} \rho_0^{(k)} \left(z_{k+1} - z_k \right) \tag{17a}$$

$$I_1 = \frac{1}{2} \sum_{k=1}^{N} \rho_0^{(k)} \left(z_{k+1}^2 - z_k^2 \right) \tag{17b}$$

$$I_2 = \frac{1}{3} \sum_{k=1}^{N} \rho_0^{(k)} \left(z_{k+1}^3 - z_k^3 \right) \tag{17c}$$

For completeness, the proper boundary conditions for all possible support types used in a rectangular laminated composite plate, as illustrated in Fig. 1, are now specified:

$$x = 0, a: \quad v_0 = w_0 = \phi_y = N_{xx} = M_{xx} = 0 \qquad \text{on } \Gamma_{S1} \tag{18a}$$

$$u_0 = w_0 = \phi_y = N_{xy} = M_{xx} = 0 \qquad \text{on } \Gamma_{S2} \tag{18b}$$

$$N_{xx} = N_{xy} = M_{xx} = M_{xy} = Q_x = 0 \qquad \text{on } \Gamma_{F} \tag{18c}$$

$$u_0 = v_0 = w_0 = \phi_x = \phi_y = 0 \qquad \text{on } \Gamma_{C} \tag{18d}$$

$$y = 0, b: \quad u_0 = w_0 = \phi_x = N_{yy} = M_{yy} = 0 \qquad \text{on } \Gamma_{S1} \tag{19a}$$

$$v_0 = w_0 = \phi_x = N_{xy} = M_{yy} = 0 \qquad \text{on } \Gamma_{S2} \tag{19b}$$

$$N_{yy} = N_{xy} = M_{yy} = M_{xy} = Q_y = 0 \qquad \text{on } \Gamma_{F} \tag{19c}$$

$$u_0 = v_0 = w_0 = \phi_x = \phi_y = 0 \qquad \text{on } \Gamma_{C} \tag{19d}$$

Clearly, combinations of the boundary conditions in Eqs. (18) and (19) can be made, in view of the support types considered for each of the four edges of the rectangular laminate. The notation used hereafter for the boundary conditions is such that each edge is specified as simply supported (S), free (F) or clamped (C), strictly in this sequence: $x = 0$, $x = a$, $y = 0$ and $y = b$. For simply supported boundary conditions two types of support are possible, usually named S1 and S2. Whichever is being used is specified in the end. Hence, the notation FFSS1 for example, is used to denote a rectangular laminate for which the edges $x = 0, a$ are free and the edges $y = 0, b$ are simply supported of type 1.

2.3 Least-Squares Formulation

From a practical standpoint, it is best to develop a least-squares finite element model that allows the use of C^0 basis functions in order to reduce the higher regularity requirements of any weighted residual formulation (see Pontaza [9]). Therefore, whenever necessary the governing equations should be transformed into an equivalent first-order system, which implies that additional independent variables need to be introduced. Nonetheless, this transformation can be argued to be somewhat beneficial, as the auxiliary variables may represent physically meaningful variables, in the framework of mixed formulations. In the present case though, both systems of governing equations are already of first-order, namely the system given by Eqs. (1)-(6) for static

analysis and the system given by Eqs. (7)-(12) for free vibration analysis. Hence, it is only necessary to develop the least-squares functional appropriate to each analysis and minimize it with respect to the chosen approximation spaces to obtain the correspondent least-squares finite element model.

Basically, the least-squares functional is defined by measuring the residuals of the governing equations in terms of suitable norms. To do so, standard notation is used. Specifically, the norm corresponding to the Sobolev space $H^s(\Omega)$, $s \geq 0$ is denoted by $\|\cdot\|_{s,\Omega}$ and $\mathbf{H}^s(\Omega)$ represents the product space $\left[H^s(\Omega)\right]^n$, where n is the number of space dimensions.

Thus, the least-squares functional for the static analysis of laminated composite plates is based on the norms of Eqs. (1)-(6), as follows:

$$\begin{aligned} J_S(\mathbf{u},w,\boldsymbol{\Phi},\mathbf{N},\mathbf{M},\mathbf{Q};q) = \tfrac{1}{2}\Big(& \left\| \underline{\partial}_\varepsilon^{\mathrm{T}}\mathbf{N} \right\|_{0,\Omega}^2 + \left\| \nabla\cdot\mathbf{Q} + q \right\|_{0,\Omega}^2 + \\ & + \left\| \underline{\partial}_\varepsilon^{\mathrm{T}}\mathbf{M} - \mathbf{Q} \right\|_{0,\Omega}^2 + \left\| \mathbf{N} - \underline{\mathbf{A}}\,\underline{\partial}_\varepsilon\mathbf{u} - \underline{\mathbf{B}}\,\underline{\partial}_\varepsilon\boldsymbol{\Phi} \right\|_{0,\Omega}^2 + \\ & + \left\| \mathbf{M} - \underline{\mathbf{B}}\,\underline{\partial}_\varepsilon\mathbf{u} - \underline{\mathrm{D}}\,\underline{\partial}_\varepsilon\boldsymbol{\Phi} \right\|_{0,\Omega}^2 + \left\| \mathbf{Q} - \underline{\hat{\mathbf{A}}}(\nabla w + \boldsymbol{\Phi}) \right\|_{0,\Omega}^2 \Big) \end{aligned} \tag{20}$$

Similarly, the least-squares functional for free vibration analysis is, in turn, based on the norms of Eqs. (7)-(12), as follows:

$$\begin{aligned} J_V(\mathbf{u},w,\boldsymbol{\Phi},\mathbf{N},\mathbf{M},\mathbf{Q};\omega) = \tfrac{1}{2}\Big(& \left\| \underline{\partial}_\varepsilon^{\mathrm{T}}\mathbf{N} + \omega^2 I_0\mathbf{u} + \omega^2 I_1\boldsymbol{\Phi} \right\|_{0,\Omega}^2 + \\ & + \left\| \nabla\cdot\mathbf{Q} + \omega^2 I_0 w \right\|_{0,\Omega}^2 + \left\| \underline{\partial}_\varepsilon^{\mathrm{T}}\mathbf{M} - \mathbf{Q} + \omega^2 I_1\mathbf{u} + \omega^2 I_2\boldsymbol{\Phi} \right\|_{0,\Omega}^2 + \\ & + \left\| \mathbf{N} - \underline{\mathbf{A}}\,\underline{\partial}_\varepsilon\mathbf{u} - \underline{\mathbf{B}}\,\underline{\partial}_\varepsilon\boldsymbol{\Phi} \right\|_{0,\Omega}^2 + \left\| \mathbf{M} - \underline{\mathbf{B}}\,\underline{\partial}_\varepsilon\mathbf{u} - \underline{\mathrm{D}}\,\underline{\partial}_\varepsilon\boldsymbol{\Phi} \right\|_{0,\Omega}^2 + \\ & + \left\| \mathbf{Q} - \underline{\hat{\mathbf{A}}}(\nabla w + \boldsymbol{\Phi}) \right\|_{0,\Omega}^2 \Big) \end{aligned} \tag{21}$$

Accordingly, the least-squares principle can be stated as:
Find $(\mathbf{u},w,\boldsymbol{\Phi},\mathbf{N},\mathbf{M},\mathbf{Q}) \in X$ such as for all $(\mathbf{s},t,\boldsymbol{\Psi},\mathbf{O},\mathbf{P},\mathbf{R}) \in X$

$$J_S(\mathbf{u},w,\boldsymbol{\Phi},\mathbf{N},\mathbf{M},\mathbf{Q};q) \leq J_S(\mathbf{s},t,\boldsymbol{\Psi},\mathbf{O},\mathbf{P},\mathbf{R};q), \text{ if static analysis} \tag{22}$$

$$J_V(\mathbf{u},w,\boldsymbol{\Phi},\mathbf{N},\mathbf{M},\mathbf{Q};\omega) \leq J_V(\mathbf{s},t,\boldsymbol{\Psi},\mathbf{O},\mathbf{P},\mathbf{R};\omega), \text{ if free vibration analysis} \tag{23}$$

The space X is defined below and satisfies the support type boundary conditions:

$$X = \left\{ (\mathbf{u},w,\boldsymbol{\Phi},\mathbf{N},\mathbf{M},\mathbf{Q}) \in \mathbf{H}^1(\Omega)\times H^1(\Omega)\times\mathbf{H}^1(\Omega)\times\mathbf{H}^1(\Omega)\times\mathbf{H}^1(\Omega)\times\mathbf{H}^1(\Omega) \right\} \tag{24}$$

Hence, the least-squares formulation leads the static and free vibration analysis of laminated composite plates to the unconstrained minimization problems given by Eq. (22) and Eq. (23), respectively. Subsequently, the finite element models are developed by minimizing the least-

squares functional. Specifically, the Euler-Lagrange equations are derived for each minimization problem, so as to obtain the least-squares variational problem for static and free vibration analysis.

2.4 Finite Element Models

The mentioned least-squares variational problems give rise to the corresponding finite element models for static and free vibration analysis of laminated composite plates. Accordingly, the infinite dimensional space X is now restricted to the finite-dimensional subspace X_{hp}, where h denotes the mesh parameter and p the order for the variables basis functions.
Ultimately, the mixed least-squares finite element model for static analysis takes the following matrix form:

$$\begin{bmatrix} K_{ij}^{uu} & \cdots & K_{ij}^{uQ_y} \\ \vdots & \ddots & \vdots \\ K_{ji}^{uQ_y} & \cdots & K_{ij}^{Q_yQ_y} \end{bmatrix} \begin{Bmatrix} u_j \\ \vdots \\ Q_{y\,j} \end{Bmatrix} = \begin{Bmatrix} F_i^u \\ \vdots \\ F_i^{Q_y} \end{Bmatrix} \tag{25}$$

In addition, the mixed least-squares model for free vibration analysis develops into a quadratic eigenvalue problem as follows, also in matrix form:

$$\left(\begin{bmatrix} K_{ij}^{uu} & \cdots & K_{ij}^{uQ_y} \\ \vdots & \ddots & \vdots \\ K_{ji}^{uQ_y} & \cdots & K_{ij}^{Q_yQ_y} \end{bmatrix} + \omega^2 \begin{bmatrix} C_{ij}^{uu} & \cdots & C_{ij}^{uQ_y} \\ \vdots & \ddots & \vdots \\ C_{ji}^{uQ_y} & \cdots & C_{ij}^{Q_yQ_y} \end{bmatrix} + \omega^4 \begin{bmatrix} M_{ij}^{uu} & \cdots & M_{ij}^{uQ_y} \\ \vdots & \ddots & \vdots \\ M_{ji}^{uQ_y} & \cdots & M_{ij}^{Q_yQ_y} \end{bmatrix} \right) \begin{Bmatrix} u_j \\ \vdots \\ Q_{y\,j} \end{Bmatrix} = \begin{Bmatrix} 0 \\ \vdots \\ 0 \end{Bmatrix} \tag{26}$$

Both finite element models yield only symmetric matrices by means of the least-squares formulation. Specifically, in view of the adopted FSDT mixed formulation, all matrices can be structured in 13×13 submatrices by considering the variables separately: namely, the 5 generalized displacements and the 8 stress resultants. The explicit integral expressions of all nonzero submatrices K_{ij}, C_{ij} and M_{ij} and all nonzero subvectors F_i are included in Appendix A.
The stiffness matrix K is shared by both models and it is not only symmetric but also positive-definite, once the boundary conditions are properly imposed. This fact allows the use of robust solvers for the static analysis of laminated composite plates by the mixed least-squares model. In the quadratic eigenvalue problem, besides the stiffness matrix K, both C and M appear as indeed mass matrices. The difference is that the matrix M refers to the mass relation among generalized displacements only, whereas the matrix C translates the mass coupling between generalized displacements and stress resultants.

In view of the finite element method, the approach for numerically evaluating the integrals implicit in Eqs. (25) and (26) is to map the finite elements that form the entire model into a master element. For both least-squares models implemented, the integrals are evaluated using full integration through Gauss quadrature rules, which implies a master element with the coordinate system: $-1 \le (\xi, \eta) \le 1$. Over this master element, the variables are approximated by equal high-order C^0 basis functions as exemplified for the transverse deflection below:

$$w_0(\xi,\eta) \approx w_0^{hp}(\xi,\eta) = \sum_{j=1}^{n} w_j \varphi_j^w(\xi,\eta) \tag{27}$$

Here, w_j denotes nodal values for the transverse deflection, φ_j^w the associated high-order C^0 basis functions and n the number of nodes in the finite element.

Specifically, the mixed least-squares model for static analysis uses the classical C^0 Lagrange basis functions, whereas the later model for free vibration analysis uses instead C^0 interpolant polynomials of Gauss-Lobatto-Legendre quadrature points. The last basis functions were initially used in the spectral element method and are in fact more suitable for high-order finite elements. In any case, the two-dimensional basis functions are given by tensor products of the corresponding one-dimensional basis functions.

The well-known one-dimensional Lagrange basis functions of order $p = N$-1 can be defined by N equally spaced nodes ξ_i, given $\xi_1 = -1$ and $\xi_N = 1$, as follows:

$$\varphi_i(\xi) = \prod_{\substack{j=1 \\ j \neq i}}^{N} \frac{\xi - \xi_j}{\xi_i - \xi_j} \tag{28}$$

Alternatively, the one-dimensional basis functions derived from Gauss-Lobatto-Legendre points of order $p = N$-1, can be written using the Legendre polynomial of same order P_{N-1}, as follows:

$$\varphi_i(\xi) = -\frac{\left(1-\xi^2\right)P'_{N-1}(\xi)}{N(N-1)P_{N-1}(\xi_i)(\xi - \xi_i)} \tag{29}$$

where, ξ_i represents N nodes now given by the roots of $\left(1-\xi^2\right)P'_{N-1}(\xi) = 0$ in the interval [-1,1]. For more details on these basis functions see Warburton et al [14].

Furthermore, the implemented least-squares models for static and free vibration analysis differ also in the Gauss quadrature rule used. Gauss-Legendre rule is used for static analysis, whereas Gauss-Lobatto-Legendre rule is conveniently employed for free vibration analysis, due to the chosen basis functions.

The global system of equations either for static or free vibration analysis is then assembled from the element contributions by the standard summation approach, followed by imposition of the appropriate boundary conditions (see Reddy [6]). In fact, unlike weak form finite element models that allow weak imposition of stress resultants by integral boundary terms, the least-squares models only allow strong imposition of the boundary conditions both for stress resultants and generalized displacements.

2.5 Computational Specifics

The mixed least-squares model for static analysis of laminated composite plates yields a symmetric and positive-definite system of algebraic equations. Hence, its numerical solution is in fact straightforward. However, post-computation of strains and stresses such that no numerical differentiation is carried out requires a more attentive procedure.

In detail, the membrane and flexural strains are computed first using the following laminate constitutive relations, once the solution of stress resultants is known:

$$\begin{Bmatrix} \mathbf{N} \\ \mathbf{M} \end{Bmatrix} = \begin{bmatrix} \underline{\mathbf{A}} & \underline{\mathbf{B}} \\ \underline{\mathbf{B}} & \underline{\mathbf{D}} \end{bmatrix} \begin{Bmatrix} \boldsymbol{\varepsilon}^0 \\ \boldsymbol{\varepsilon}^1 \end{Bmatrix}, \; \mathbf{Q} = \underline{\hat{\mathbf{A}}}\, \hat{\boldsymbol{\varepsilon}}^0 \tag{30}$$

In these equations, the implied vector form for the stress resultants is previously defined in Eq. (13) and the matrix form for the laminate stiffnesses is given by Eq. (15). Hence, only the appropriate form for the strain components needs to be specified, as follows:

$$\boldsymbol{\varepsilon}^0 = \begin{bmatrix} \varepsilon_{xx}^0 & \varepsilon_{yy}^0 & \gamma_{xy}^0 \end{bmatrix}^{\mathrm{T}}, \; \boldsymbol{\varepsilon}^1 = \begin{bmatrix} \varepsilon_{xx}^1 & \varepsilon_{yy}^1 & \gamma_{xy}^1 \end{bmatrix}^{\mathrm{T}}, \; \hat{\boldsymbol{\varepsilon}}^0 = \begin{bmatrix} \gamma_{xz}^0 & \gamma_{yz}^0 \end{bmatrix}^{\mathrm{T}} \tag{31}$$

Secondly, the in-plane and transverse stresses are computed given the prior membrane and flexural strains, again through the laminate constitutive relations but yet in another form:

$$\boldsymbol{\sigma}^{(k)} = \underline{\mathbf{Q}}^{(k)} \left(\boldsymbol{\varepsilon}^0 + z\, \boldsymbol{\varepsilon}^1 \right), \; \hat{\boldsymbol{\sigma}}^{(k)} = \underline{\hat{\mathbf{Q}}}^{(k)}\, \hat{\boldsymbol{\varepsilon}}^0 \tag{32}$$

Specifically, the in-plane stresses are computed on the top and bottom of each *k*th layer while the transverse stresses are only computed within each *k*th layer, in agreement with the FSDT stress variations through the laminate thickness. For clearness, in the previous equations, it is considered the following matrix form for the lamina stiffnesses:

$$\underline{\mathbf{Q}}^{(k)} = \begin{bmatrix} \overline{Q}_{11} & \overline{Q}_{12} & \overline{Q}_{16} \\ \overline{Q}_{12} & \overline{Q}_{22} & \overline{Q}_{26} \\ \overline{Q}_{16} & \overline{Q}_{26} & \overline{Q}_{66} \end{bmatrix}^{(k)}, \; \underline{\hat{\mathbf{Q}}}^{(k)} = \begin{bmatrix} \overline{Q}_{55} & \overline{Q}_{45} \\ \overline{Q}_{45} & \overline{Q}_{44} \end{bmatrix}^{(k)} \tag{33}$$

Additionally, the stress components are defined in a similar manner as the strains components before, as follows:

$$\boldsymbol{\sigma}^{(k)} = \begin{bmatrix} \sigma_{xx}^{(k)} & \sigma_{yy}^{(k)} & \sigma_{xy}^{(k)} \end{bmatrix}^{\mathrm{T}}, \; \hat{\boldsymbol{\sigma}}^{(k)} = \begin{bmatrix} \sigma_{xz}^{(k)} & \sigma_{yz}^{(k)} \end{bmatrix}^{\mathrm{T}} \tag{34}$$

The post-computation described for static analysis of laminated composite plates ensures that the computed stresses experience no loss of accuracy through differentiation and are evaluated in nodal points as any other variable.

Regarding the free vibration analysis of laminated composite plates, the mixed least-squares model yields a quadratic eigenvalue problem involving symmetric matrices. Since numerical algorithm design for quadratic eigenproblems is still an active research topic, the main endeavor is to pursue an efficient method to solve the quadratic eigenproblem under consideration.

One approach is to use methods that tackle the quadratic eigenproblem directly, usually variants of Newton's method that find one eigenpair at a time. However, the availability of such methods is rather deficient. The approach actually chosen is to transform the quadratic eigenproblem into an equivalent "linear" generalized eigenproblem to allow the use of traditional methods for solution of eigenvalue problems (see Bai et al [15]). These methods are in fact widely available. In detail, the current implementation uses ARPACK subroutines, which have a

long proven robustness and accuracy, to compute a few eigenvalues and eigenvectors with Implicitly Restarted Arnoldi Methods (IRAM).
Specifically, the assembled quadratic eigenvalue problem is of the following form:

$$\left([K]+\lambda[C]+\lambda^2[M]\right)\{\Delta\}=\{0\},\ \lambda=\omega^2 \tag{35}$$

For reasons soon made clear, an invert spectral transformation is first considered, as follows:

$$\left([M]+\mu[C]+\mu^2[K]\right)\{\Delta\}=\{0\},\ \mu=1/\lambda \tag{36}$$

Then, the desired transformation into an equivalent generalized eigenproblem takes the form specified below:

$$[A]\{x\}=\mu[B]\{x\} \tag{37}$$

where,

$$[A]=\begin{bmatrix}0 & I\\ -M & -C\end{bmatrix},\ [B]=\begin{bmatrix}I & 0\\ 0 & K\end{bmatrix},\ \{x\}=\begin{Bmatrix}\Delta\\ \mu\Delta\end{Bmatrix} \tag{38}$$

Ultimately, this approach reduces the original quadratic eigenproblem into a non-symmetric generalized eigenproblem, where the matrix *B* is still symmetric and positive-definite. In fact, the reason for the prior invert transformation is to ensure that the matrix *B* is positive-definite by depending on the stiffness matrix *K* rather than the mass matrix *M* (besides the identity matrix *I*).
Considering the above transformations, the equivalent generalized eigenproblem can be efficiently solved by ARPACK subroutines. In addition, the few computed eigenvalues and eigenvectors of the equivalent eigenproblem must then be used to obtain the eigenvalues and eigenvectors of the original quadratic eigenproblem through the relations above.
Finally, the specific nature of the finite element matrices *K*, *C* and *M*, render the quadratic eigenproblem and the equivalent generalized eigenproblem generally complex solutions. However, once the original eigenvalues and eigenvectors are recovered, the complex solutions (in conjugate pairs) show a negligible imaginary part relatively to the real counterpart. So, for practical purposes, only the real part of the solution of free vibration analysis of laminated composite plates is reported in the following numerical examples.

2.6 Numerical Examples

The predictive capabilities of the proposed mixed least-squares models are now demonstrated through selected problems of static and free vibration analysis of laminated composite plates.
Specifically, four square laminated composite plates are considered with different boundary conditions and a range of side-to-thickness ratios, covering thick to thin laminates. The particular laminates under analysis are two cross-ply laminates (0/90) and (0/90/0/90/0) and two angle-ply laminates (-45/45) and (30/-60/60/-30). In addition, the selected problems of static analysis concern laminated composite plates under a uniformly distributed load of intensity q_0.

The material properties for all layers of the given laminates are assumed to be the same, as shown:

$$E_1/E_2 = 25,\ G_{12} = G_{13} = 0.5E_2,\ G_{23} = 0.2E_2,\ \nu_{12} = 0.25 \tag{39}$$

Moreover, the subsequent numerical results both in graphical and tabular forms for the main variables are nondimensionalized, as specified below:

$$\overline{w} = w_0\left(\frac{E_2 h^3}{a^4 q_0}\right)\times 10^2,\ \overline{\mathbf{M}} = \mathbf{M}\frac{10}{a^2 q_0},\ \overline{\mathbf{Q}} = \mathbf{Q}\frac{10}{a q_0} \tag{40a}$$

$$\overline{\boldsymbol{\sigma}}^{(k)} = \boldsymbol{\sigma}^{(k)}\left(\frac{h^2}{a^2 q_0}\right),\ \overline{\hat{\boldsymbol{\sigma}}}^{(k)} = \hat{\boldsymbol{\sigma}}^{(k)}\left(\frac{h}{a q_0}\right) \tag{40b}$$

$$\overline{\omega} = \omega\left(\frac{a^2}{h}\right)\sqrt{\frac{\rho}{E_2}} \tag{41}$$

Analytical solutions are also presented alongside the numerical results for comparison. Basically, the well-known FSDT Navier solutions or Lévy solutions for static or free vibration analysis of laminated composite plates are reported, according to the problem under analysis (see Reddy [7]). For static analysis, the Navier series are evaluated for $m,n = 1,...,40$ and the Lévy series for $n = 1,...,40$.

Cross-ply laminates

The first selected problem is the static analysis of the antisymmetric laminate (0/90) with SSSS1 boundary conditions. A uniform mesh of 4×4 square elements is used to model the composite plate and an increasing order for the mixed least-squares element is considered. Specifically, 4th, 6th and 8th-order elements are successively applied in order to investigate the *p*-convergence of the proposed model. The computed results are summarized in Table 1.

Table 1. Static results for the laminate (0/90) SSSS1 using a uniform mesh 4×4.

a/h	p-order	$\overline{w}\left(\frac{a}{2},\frac{a}{2}\right)$	$\overline{M}_{yy}\left(\frac{a}{2},\frac{a}{2}\right)$	$\overline{M}_{xy}(0,0)$	$\overline{Q}_y\left(\frac{a}{2},0\right)$	$\overline{\sigma}_{yy}^{(2t)}\left(\frac{a}{2},\frac{a}{2}\right)$	$\overline{\sigma}_{xy}^{(1b)}(0,0)$	$\overline{\sigma}_{xz}^{(1)}\left(0,\frac{a}{2}\right)$
10	4	1.9469	0.6265	-0.1621	3.4675	1.0712	0.0973	0.5944
	6	1.9469	0.6268	-0.1605	3.4698	1.0716	0.0963	0.5948
	8	1.9469	0.6268	-0.1604	3.4703	1.0716	0.0962	0.5949
	Analytical	1.9469	0.6268	-0.1603	3.4194	1.0716	0.0962	0.5862
20	4	1.7583	0.6288	-0.1609	3.4801	1.0745	0.0965	0.5966
	6	1.7582	0.6291	-0.1580	3.4883	1.0748	0.0948	0.5980
	8	1.7582	0.6291	-0.1576	3.4880	1.0748	0.0946	0.5979
	Analytical	1.7582	0.6290	-0.1575	3.4369	1.0748	0.0945	0.5892
100	4	1.6980	0.6297	-0.1621	3.4560	1.0757	0.0973	0.5924
	6	1.6980	0.6301	-0.1571	3.4938	1.0762	0.0943	0.5989
	8	1.6981	0.6301	-0.1561	3.4936	1.0763	0.0937	0.5989
	Analytical	1.6980	0.6300	-0.1558	3.4427	1.0762	0.0935	0.5902

The effect of mesh refinement is examined as well using only 4th-order elements and a uniform mesh of 4×4, 5×5 and 8×8 square elements. These numerical results are in turn shown in Table 2. Both tables include the results for transverse deflection, stress resultants and stresses, considering side-to-thickness ratios of 10, 20 and 100. In particular, for all stress results tabulated henceforth the right superscript specifies the layer where the results are referred to and when necessary also the bottom or top interface by *b* or *t*, respectively. Furthermore, Navier analytical solutions for this problem are shown throughout both tables.

Table 2. Static results for the laminate (0/90) SSSS1 using the 4th-order element.

a/h	Mesh	$\overline{w}\left(\frac{a}{2},\frac{a}{2}\right)$	$\overline{M}_{yy}\left(\frac{a}{2},\frac{a}{2}\right)$	$\overline{M}_{xy}(0,0)$	$\overline{Q}_{y}\left(\frac{a}{2},0\right)$	$\overline{\sigma}_{yy}^{(2t)}\left(\frac{a}{2},\frac{a}{2}\right)$	$\overline{\sigma}_{xy}^{(1b)}(0,0)$	$\overline{\sigma}_{xz}^{(1)}\left(0,\frac{a}{2}\right)$
10	4×4	1.9469	0.6265	-0.1621	3.4675	1.0712	0.0973	0.5944
	5×5	1.9469	0.6268	-0.1612	3.4709	1.0716	0.0967	0.5950
	8×8	1.9469	0.6267	-0.1605	3.4707	1.0716	0.0963	0.5950
	Analytical	1.9469	0.6268	-0.1603	3.4194	1.0716	0.0962	0.5862
20	4×4	1.7583	0.6288	-0.1609	3.4801	1.0745	0.0965	0.5966
	5×5	1.7583	0.6291	-0.1594	3.4886	1.0748	0.0957	0.5980
	8×8	1.7582	0.6290	-0.1580	3.4882	1.0748	0.0948	0.5980
	Analytical	1.7582	0.6290	-0.1575	3.4369	1.0748	0.0945	0.5892
100	4×4	1.6980	0.6297	-0.1621	3.4560	1.0757	0.0973	0.5924
	5×5	1.6980	0.6300	-0.1598	3.4968	1.0762	0.0959	0.5995
	8×8	1.6980	0.6300	-0.1572	3.4926	1.0762	0.0943	0.5987
	Analytical	1.6980	0.6300	-0.1558	3.4427	1.0762	0.0935	0.5902

Overall, the numerical results in Tables 1 and 2 are in good agreement with the analytical solutions for the entire range of side-to-thickness ratios analyzed. In fact, the centre transverse deflection is rightly predicted using just 4th-order elements even when a thin laminate is considered (with a side-to-thickness ratio of 100). Most notably, convergence towards the analytical solution is verified, either with *p*- or *h*-refinements, as should be expected. Actually, an exact study on the asymptotic behaviour of mixed finite elements based on least-squares formulation can be found in Pontaza [9]. In the case of the transverse force resultant and transverse stress, it is noted a slight discrepancy between the analytical and numerical results, which is believed to be due to a not as accurate analytical representation.

In Fig. 2, it is shown the predictive distributions of the in-plane stresses σ_{yy} and σ_{xy} along the laminate thickness, using a side-to-thickness ratio of 10. The proper Navier solution is plotted alongside the numerical results obtained with the 8th-order element in a 4×4 mesh.

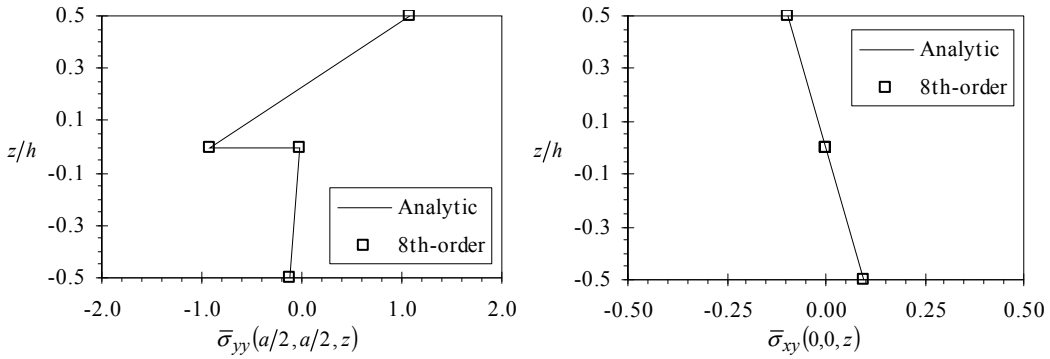

Figure 2. In-plane stresses for the laminate (0/90) SSSS1 with $a/h = 10$.

Continuing the analysis of the same antisymmetric laminate (0/90) with SSSS1 boundary conditions, the problem of free vibration is considered next. In this case, a uniform mesh of 4×4 square elements is used together with the 4th-order mixed least-squares element. The results for the fundamental frequency using the same side-to-thickness ratios as before are presented in Table 3, along with the Navier solutions.

Table 3. Free vibration results for the laminate (0/90) SSSS1 using a uniform mesh 4×4.

a/h	p-order	$\overline{\omega}_1$
10	4	8.9006
	Analytical	8.9001
20	4	9.4746
	Analytical	9.4745
100	4	9.6873
	Analytical	9.6873

As mentioned earlier, the mixed least-squares model for free vibration analysis yields a quadratic eigenproblem, that to be later solved by ARPACK subroutines requires an invert spectral transformation followed by another transformation into an equivalent generalized eigenproblem. With this mind, the smaller eigenvalues of the original quadratic eigenproblem correspond to the larger eigenvalues of the generalized eigenproblem. Hence, to compute the lower natural frequencies of the quadratic eigenproblem, it is specified to ARPACK to extract the eigenvalues of largest real part. Specifically, the results in Table 3 are obtained by specifying the extraction of 2 eigenvalues (which come as a complex conjugate pair) using 50 Arnoldi basis vectors. In fact, the choice of both these numbers for an optimal performance of ARPACK is truly problem dependent. Since this optimum choice was not investigated, whenever free vibration results are presented the number of eigenvalues requested and number of Arnoldi basis vectors used are explicitly stated.

Returning to Table 3, the computed fundamental frequencies are remarkably in agreement with the analytical solutions, for all side-to-thickness ratios considered. In fact, the

4th-order mixed least-squares element appears to be quite sufficient to obtain very goods results for the fundamental frequency in this case.

The next problem is the static analysis of the symmetric laminate (0/90/0/90/0) with FFSS1 boundary conditions. Once more, *p*-convergence of the proposed mixed least-squares element is inspected, using in turn 4th, 6th and 8th-order elements in a uniform mesh of 4×4 square elements. Table 4 shows the results for the transverse deflection, stress resultants and stresses, using again side-to-thickness ratios of 10, 20 and 100. For this problem, Lévy analytical solutions are presented for comparison.

Table 4. Static results for the laminate (0/90/0/90/0) FFSS1 using a uniform mesh 4×4.

a/h	p-order	$\overline{w}\left(\frac{a}{2},\frac{a}{2}\right)$	$\overline{M}_{xx}\left(\frac{a}{2},\frac{a}{2}\right)$	$\overline{M}_{yy}\left(\frac{a}{2},\frac{a}{2}\right)$	$\overline{Q}_{y}\left(\frac{a}{2},0\right)$	$\overline{\sigma}_{xx}^{(4t)}\left(\frac{a}{2},\frac{a}{2}\right)$	$\overline{\sigma}_{yy}^{(4t)}\left(\frac{a}{2},\frac{a}{2}\right)$	$\overline{\sigma}_{yz}^{(4)}\left(\frac{a}{2},0\right)$
10	4	3.0600	0.0061	1.2458	4.9787	0.0179	1.8719	0.9335
	6	3.0600	0.0061	1.2458	4.9785	0.0179	1.8718	0.9335
	8	3.0600	0.0061	1.2458	4.9785	0.0179	1.8718	0.9335
	Analytical	3.0600	0.0061	1.2458	4.9279	0.0179	1.8718	0.9240
20	4	2.7082	0.0069	1.2449	4.9770	0.0179	1.8705	0.9332
	6	2.7082	0.0070	1.2449	4.9750	0.0179	1.8706	0.9328
	8	2.7082	0.0069	1.2449	4.9748	0.0179	1.8705	0.9336
	Analytical	2.7082	0.0069	1.2449	4.9241	0.0179	1.8705	0.9233
100	4	2.5956	0.0072	1.2446	4.9787	0.0179	1.8700	0.9335
	6	2.5957	0.0073	1.2446	4.9792	0.0179	1.8701	0.9336
	8	2.5955	0.0074	1.2446	4.9783	0.0179	1.8701	0.9334
	Analytical	2.5957	0.0074	1.2446	4.9230	0.0179	1.8701	0.9231

Noticeably, the computed numerical results in Table 4 show excellent agreement with the analytical solutions, even more than in the previous static problem. Not only the centre transverse deflection, but also stress resultants and stresses can be predicted exactly using just 4th-order elements, for all side-to-thickness ratios considered. Basically, it seems that most of the computed results are converged using the 4th-order elements, including the results for a thin laminate. Again, only the transverse force resultant and transverse stress show a small discrepancy between the analytical and numerical results. This occurrence is more or less apparent throughout every static analysis problems here presented. So, to avoid repetition, it is understood henceforth that the static analytical solutions for these variables may not be fully converged in the series representation.

Fig. 3 shows the distributions for the in-plane stresses σ_{xx} and σ_{yy} through the laminate thickness, using a side-to-thickness ratio of 10. These plots contain the numerical results by the 8th-order element in a 4×4 mesh with the Lévy solution.

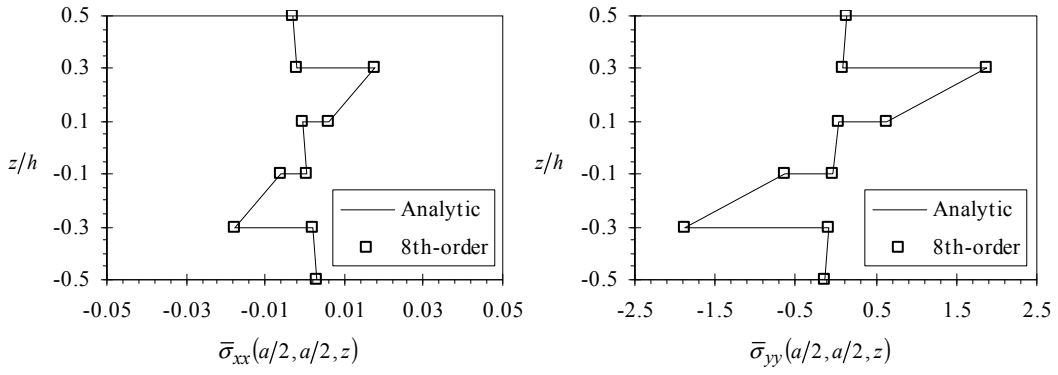

Figure 3. In-plane stresses for the laminate (0/90/0/90/0) FFSS1 with $a/h = 10$.

To conclude the static analysis of both cross-ply laminates previously considered, the transverse deflections along the line $x = a/2$ of the plate are plotted in Fig. 4. Namely, the antisymmetric laminate (0/90) SSSS1 and the symmetric laminate (0/90/0/90/0) FFSS1. Fig. 4 contains then, the corresponding analytical solutions and numerical results using the 6th-order element in a 4×4 mesh, given side-to-thickness ratios of 10 and 100 (*i.e.* for thick and thin laminates, respectively).

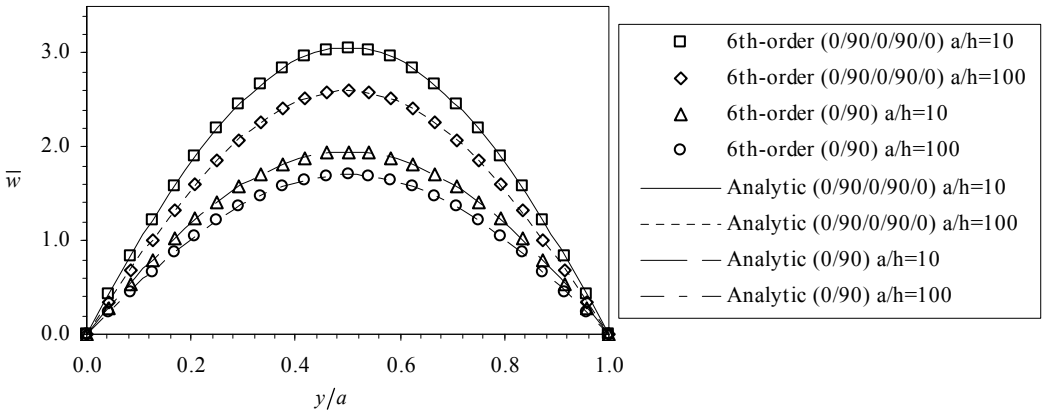

Figure 4. Transverse deflections along $x = a/2$ for the cross-ply laminates.

Evidently, Fig. 4 demonstrates that the computed results by the proposed mixed least-squares element for static analysis are in any case well in agreement with the analytical solutions, whether thin or thick laminates are concerned. In fact, results so far suggest that this mixed least-squares model is insensitive to shear locking, at least for the *p*-levels considered.

The last selected problem of this section devoted to cross-ply laminates is the free vibration analysis of the former symmetric laminate (0/90/0/90/0), but with SSSS2 boundary conditions instead. This time, the 5 lowest natural frequencies are investigated using a uniform mesh of 4×4 square elements and the 4th-order mixed least-squares element. The numerical results for these natural frequencies are given in Table 5 for the usual side-to-thickness ratios, along with the Navier solutions. In particular, this computation uses ARPACK to extract of a cluster of 14 eigenvalues (in complex conjugate pairs) with 57 Arnoldi basis vectors.

Table 5. Free vibration results for the laminate (0/90/0/90/0) SSSS2 using a uniform mesh 4×4.

a/h	p-order	$\overline{\omega}_1$	$\overline{\omega}_2$	$\overline{\omega}_3$	$\overline{\omega}_4$	$\overline{\omega}_5$
10	4	12.5650	24.0078	30.0457	36.5359	40.1397
	Analytical	12.5651	24.0120	30.0549	36.5559	40.1329
20	4	14.3875	29.2513	42.4381	50.1919	54.8037
	Analytical	14.3875	29.2508	42.4421	50.2606	54.8754
100	4	15.1909	31.8771	51.7589	60.3319	64.9051
	Analytical	15.1909	31.8770	51.7581	60.3285	64.9772

Overall, the 5 computed natural frequencies exhibit an outstanding accordance with the analytical solutions, regardless of the side-to-thickness ratios considered. Actually, the 4th-order element is able to predict quite well the natural frequencies higher than the fundamental frequency, even though the results slightly worsen as the natural frequencies increase (which is expected to some extent).

The following surface plots illustrate the modes of vibration computed for these 5 natural frequencies, concerning only the transverse deflection.

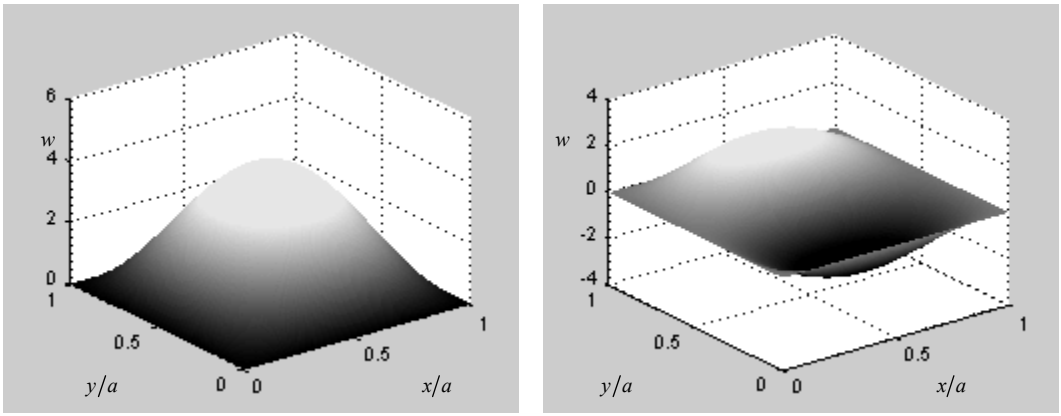

Figure 5. Modes of vibration 1 and 2 for the laminate (0/90/0/90/0) SSSS2.

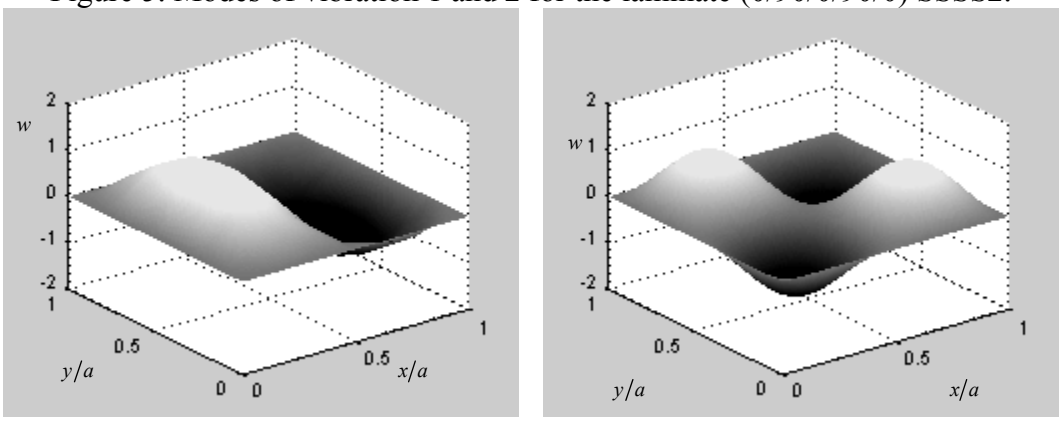

Figure 6. Modes of vibration 3 and 4 for the laminate (0/90/0/90/0) SSSS2.

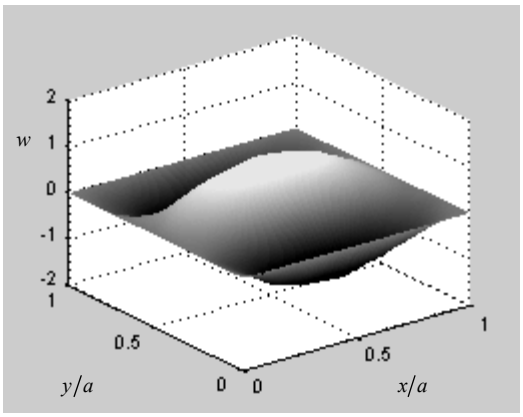

Figure 7. Mode of vibration 5 for the laminate (0/90/0/90/0) SSSS2.

The represented modes of vibration in Figs. 5-7 are also obtained using the 4th-order mixed least-squares element in a 4×4 uniform mesh and specifically for a side-to-thickness ratio of 10, although qualitatively the modes are the same for all side-to-thickness ratios. To be precise, all these graphics are constructed from the eigenvectors solution (for transverse deflection) and taking into account the 4th-order basis functions as well as the finite elements geometry transformations between the master element. So, ultimately, the overall mode shape is displayed by putting together every finite element contribution.

The modes of vibration for the transverse deflection are indeed in agreement with the Navier solutions, as the specific pair of harmonics that correspond to each analytical natural frequency matches the represented modes. Explicitly, the pair of harmonics along x and y respectively, for increasing natural frequencies are (1,1), (1,2), (2,1), (2,2) and (1,3). Therefore, the proposed mixed least-squares model for free vibration analysis based on C^0 high-order basis functions, is in fact capable of good predictions for the natural frequencies as well as the modes of vibration.

Angle-ply laminates

This section starts with the static analysis problem of the antisymmetric laminate (-45/45) with SSSS2 boundary conditions. Similarly to the first selected problem, the effect of both *p*- and *h*-refinements is examined. Table 6 shows the computed results using a fixed uniform mesh of 4×4 square elements and an increasing order for the mixed least-squares element, whereas Table 7 presents the results using a fixed *p*-level with the 4th-order element and increasingly refined meshes. Both tables include results of transverse deflection, stress resultants and stresses, with side-to-thickness ratios of 10, 20 and 100. The appropriate Navier analytical solutions are presented as well.

Table 6. Static results for the laminate (-45/45) SSSS2 using a uniform mesh 4×4.

a/h	p-order	$\overline{w}\left(\frac{a}{2},\frac{a}{2}\right)$	$\overline{M}_{yy}\left(\frac{a}{2},\frac{a}{2}\right)$	$\overline{M}_{xy}(0,0)$	$\overline{Q}_{y}\left(\frac{a}{2},0\right)$	$\overline{\sigma}_{yy}^{(2t)}\left(\frac{a}{2},\frac{a}{2}\right)$	$\overline{\sigma}_{xy}^{(1b)}(0,0)$	$\overline{\sigma}_{yz}^{(1)}\left(\frac{a}{2},0\right)$
10	4	1.2792	0.3718	-0.4417	3.2730	0.3476	0.4311	0.3928
	6	1.2792	0.3720	-0.4388	3.2778	0.3477	0.4285	0.3933
	8	1.2792	0.3720	-0.4383	3.2785	0.3478	0.4281	0.3934
	Analytical	1.2792	0.3720	-0.4379	3.2276	0.3477	0.4277	0.3873
20	4	1.0907	0.3744	-0.4500	3.2468	0.3496	0.4380	0.3896
	6	1.0907	0.3745	-0.4487	3.2507	0.3497	0.4370	0.3901
	8	1.0907	0.3745	-0.4482	3.2514	0.3497	0.4365	0.3902
	Analytical	1.0907	0.3744	-0.4477	3.2005	0.3497	0.4360	0.3841
100	4	1.0305	0.3762	-0.4547	3.2357	0.3512	0.4419	0.3883
	6	1.0305	0.3755	-0.4558	3.2392	0.3505	0.4430	0.3887
	8	1.0305	0.3743	-0.4556	3.2396	0.3505	0.4428	0.3887
	Analytical	1.0305	0.3755	-0.4549	3.1884	0.3505	0.4422	0.3826

Table 7. Static results for the laminate (-45/45) SSSS2 using the 4th-order element.

a/h	Mesh	$\overline{w}\left(\frac{a}{2},\frac{a}{2}\right)$	$\overline{M}_{yy}\left(\frac{a}{2},\frac{a}{2}\right)$	$\overline{M}_{xy}(0,0)$	$\overline{Q}_{y}\left(\frac{a}{2},0\right)$	$\overline{\sigma}_{yy}^{(2t)}\left(\frac{a}{2},\frac{a}{2}\right)$	$\overline{\sigma}_{xy}^{(1b)}(0,0)$	$\overline{\sigma}_{yz}^{(1)}\left(\frac{a}{2},0\right)$
10	4×4	1.2792	0.3718	-0.4417	3.2730	0.3476	0.4311	0.3928
	5×5	1.2792	0.3721	-0.4405	3.2798	0.3478	0.4301	0.3936
	8×8	1.2792	0.3720	-0.4391	3.2788	0.3477	0.4288	0.3935
	Analytical	1.2792	0.3720	-0.4379	3.2276	0.3477	0.4277	0.3873
20	4×4	1.0907	0.3744	-0.4500	3.2468	0.3496	0.4380	0.3896
	5×5	1.0907	0.3745	-0.4496	3.2513	0.3497	0.4377	0.3902
	8×8	1.0907	0.3744	-0.4487	3.2516	0.3497	0.4370	0.3902
	Analytical	1.0907	0.3744	-0.4477	3.2005	0.3497	0.4360	0.3841
100	4×4	1.0305	0.3762	-0.4547	3.2357	0.3512	0.4419	0.3883
	5×5	1.0305	0.3754	-0.4548	3.2355	0.3504	0.4421	0.3883
	8×8	1.0306	0.3755	-0.4551	3.2393	0.3506	0.4424	0.3887
	Analytical	1.0305	0.3755	-0.4549	3.1884	0.3505	0.4422	0.3826

Again, the numerical results shown in both Tables 6 and 7 are altogether in good agreement with the analytical solutions, for the range of side-to-thickness ratios analyzed. Specifically, convergence of the numerical results is once more verified for both *p*- and *h*-refinements. Actually, it is interesting to note that the number of degrees of freedom given by the 8th-order elements in a 4×4 mesh is exactly the same as the 4th-order elements in an 8×8 mesh. A comparison between these two cases suggests that *p*-refinement is somewhat more efficient, especially in view of side-to-thickness ratios of 10 and 20. However, for an exact study on this matter see Pontaza [9]. Still, in this problem it appears that the 4th-order element is sufficient to provide accurate predictions for the transverse deflection as well as reasonable predictions for stresses and stress resultants, whether thin or thick laminates are considered.

The in-plane stresses σ_{yy} and σ_{xy} through the laminate thickness are plotted in Fig. 8, given a side-to-thickness ratio of 10, and using the results obtained by the 8th-order element in a 4×4 mesh together with the Navier analytical solution.

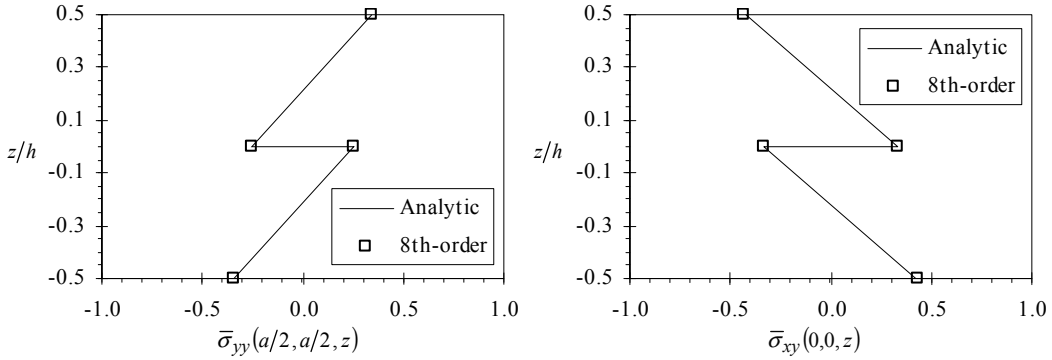

Figure 8. In-plane stresses for the laminate (-45/45) SSSS2 with $a/h = 10$.

The problem of free vibration analysis of the antisymmetric laminate (-45/45) with SSSS2 boundary is now considered. The fundamental frequency is computed by the 4th-order mixed least-squares element in a 4×4 uniform mesh, for the same side-to-thickness ratios as before. In this particular computation with ARPACK, it is specified the extraction of 2 eigenvalues (in a complex conjugate pair) using 50 Arnoldi basis vectors. The computed results are presented in Table 8 as well as the Navier solutions.

Table 8. Free vibration results for the laminate (-45/45) SSSS2 using a uniform mesh 4×4.

a/h	p-order	$\bar{\omega}_1$
10	4	10.8951
	Analytical	10.8951
20	4	11.9327
	Analytical	11.9329
100	4	12.3408
	Analytical	12.3408

From Table 8, it is verified that the computed fundamental frequencies are almost entirely coincident with the analytical solutions, for these side-to-thickness ratios. Hence, concurring with the previous free vibration analysis problems, the mixed least-squares model of 4th-order is quite capable of obtaining excellent results for the fundamental frequencies.

The very last selected problem considers the static analysis of the antisymmetric laminate (30/-60/60/-30) with SSSS2 boundary conditions. In this case, a uniform mesh of 4×4 square elements is used along with either the 4th, 6th or 8th-order elements. Table 9 shows these numerical results for the transverse deflection, stress resultants and stresses, with the usual side-to-thickness ratios. The Navier analytical solutions are likewise shown.

Table 9. Static results for the laminate (30/-60/60/-30) SSSS2 using a uniform mesh 4×4.

a/h	p-order	$\overline{w}\left(\frac{a}{2},\frac{a}{2}\right)$	$\overline{M}_{xx}\left(\frac{a}{2},\frac{a}{2}\right)$	$\overline{M}_{yy}\left(\frac{a}{2},\frac{a}{2}\right)$	$\overline{Q}_x\left(0,\frac{a}{2}\right)$	$\overline{\sigma}_{xx}^{(4t)}\left(\frac{a}{2},\frac{a}{2}\right)$	$\overline{\sigma}_{yy}^{(3t)}\left(\frac{a}{2},\frac{a}{2}\right)$	$\overline{\sigma}_{xz}^{(1)}\left(0,\frac{a}{2}\right)$
10	4	0.9261	0.7107	0.4410	3.7218	0.4702	0.4034	0.5423
	6	0.9262	0.7125	0.4419	3.7172	0.4715	0.4041	0.5416
	8	0.9262	0.7125	0.4419	3.7178	0.4714	0.4041	0.5417
	Analytical	0.9261	0.7125	0.4418	3.6668	0.4714	0.4041	0.5343
20	4	0.7306	0.7224	0.4391	3.7279	0.4785	0.3947	0.5432
	6	0.7307	0.7274	0.4413	3.7105	0.4821	0.3963	0.5407
	8	0.7307	0.7273	0.4412	3.7114	0.4821	0.3962	0.5408
	Analytical	0.7307	0.7273	0.4412	3.6604	0.4821	0.3962	0.5334
100	4	0.6671	0.7235	0.4364	3.7592	0.4796	0.3898	0.5478
	6	0.6682	0.7326	0.4413	3.7074	0.4858	0.3937	0.5402
	8	0.6681	0.7326	0.4412	3.7104	0.4858	0.3936	0.5407
	Analytical	0.6681	0.7325	0.4411	3.6594	0.4858	0.3936	0.5332

Table 9 shows yet again that the computed results are overall well in agreement with the analytical solutions. As previously stated, it is evident that even when thin laminates are considered the proposed mixed least-squares finite element experiences no shear-locking, so far as 4th- or higher-order elements are used. Nevertheless, in this particular problem the numerical results for stresses and stress resultants by the 4th-order element do not show as much accuracy as in the previous static problems, especially for a side-to-thickness ratio of 100. In fact, *p*-convergence is quite apparent when the subsequent results by the 6th-order elements are examined.

The predicted in-plane stresses σ_{xx} and σ_{yy} through the laminate thickness are plotted in the following Fig. 9, for a side-to thickness ratio of 10. Again, the stress results are given by the 8th-order element in a 4×4 uniform mesh along with the analytical solution.

Similarly to the cross-ply laminates earlier, the static analysis of both angle-ply laminates is concluded with the plot of the transverse deflections along the line $x = a/2$ of the plate, considering side-to-thickness ratios of 10 and 100. So, it is shown in the next Fig. 10 the proper transverse deflections distributions obtained by the 6th-order element in a 4×4 uniform mesh with the corresponding analytical solutions.

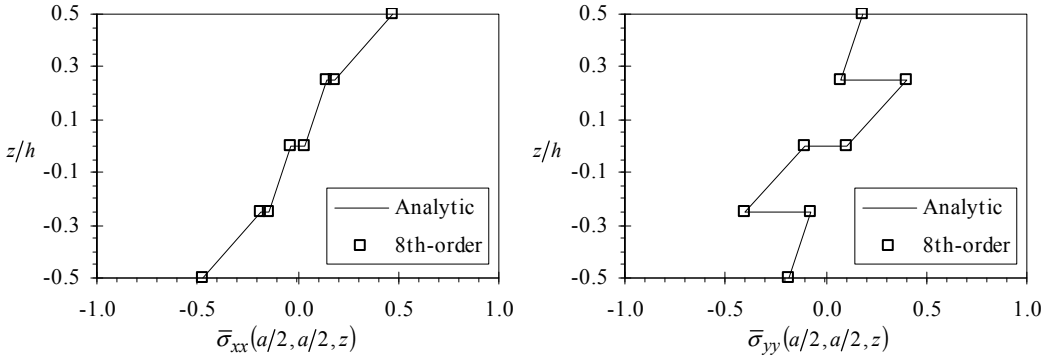

Figure 9. In-plane stresses for the laminate (30/-60/60/-30) SSSS2 with $a/h = 10$.

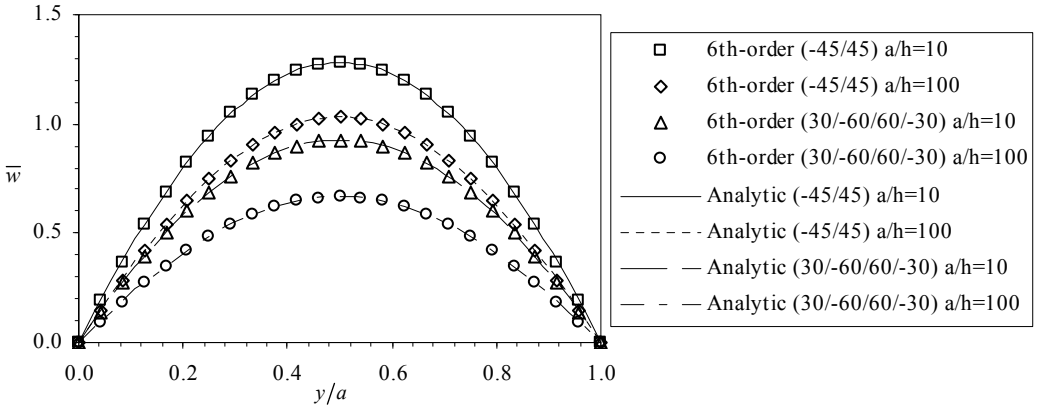

Figure 10. Transverse deflections along $x = a/2$ for the angle-ply laminates.

It is apparent in Fig. 10 that the numerical results obtained by the mixed least-squares element follow extremely well the analytical solutions, for all the cases presented. Furthermore, no evidence of shear-locking has been encountered in any static and free vibration analysis problems considered to date, intended for assessment of the proposed mixed least-squares models.

2.7 Concluding Remarks

This report presents mixed least-squares finite element models for static and free vibration analysis of laminated composite plates as a reliable alternative to the mixed weak form models. The theoretical and computational advantages of the least-squares variational principle combined with mixed formulations are stated from the start and verified for the proposed models. Explicitly, the least-squares formulation leads to an unconstrained minimization problem, which ensures that no restrictive compatibility conditions are required among the mixed finite element approximation spaces. In addition, the mixed least-squares discrete models, once the boundary conditions are duly imposed, yield a symmetric and positive-definite stiffness matrix.

The proposed mixed least-squares models for static and free vibration analysis of laminated composite plates consider the FSDT with generalized displacements and stress resultants as independent variables, using equal-order interpolation. In fact, to ensure a correct minimization of the least-squares functional, high-order C^0 basis functions and full integration are used to develop the discrete finite element models. Specifically, the model for static analysis uses the classical C^0 Lagrange basis functions and the later model for free vibration analysis uses C^0 interpolant polynomials of Gauss-Lobatto-Legendre quadrature points, which are more suitable basis functions for high-order elements.

The predictive capabilities of both mixed least-squares models are assessed by a selection of numerical examples concerning four laminated composite plates with different boundary conditions and a range of side-to-thickness ratios, from thick to thin laminates. Overall, the numerical results for static and free vibration analysis show excellent agreement with the analytical solutions for all problems examined. In the case of static analyses, results for transverse deflection, stress resultants and stresses are carefully inspected and specially, convergence of the computed results towards the analytical solutions is verified for both *p*- and

h-refinements. In free vibration analyses, the natural frequencies are remarkably well predicted and even the modes of vibration are correctly represented. Furthermore, both mixed least-squares models are shown to be insensitive to shear-locking when modeling thin laminates.

2.8 Appendix for Part 2

$$K_{ij}^{uu} = \int_{\Omega^e} \left(\left(A_{r1}^2 + B_{r1}^2\right) \frac{\partial \varphi_i^u}{\partial x} \frac{\partial \varphi_j^u}{\partial x} + \left(A_{r1}A_{r6} + B_{r1}B_{r6}\right) \left(\frac{\partial \varphi_i^u}{\partial x} \frac{\partial \varphi_j^u}{\partial y} + \frac{\partial \varphi_i^u}{\partial y} \frac{\partial \varphi_j^u}{\partial x} \right) + \right.$$

$$\left. + \left(A_{r6}^2 + B_{r6}^2\right) \frac{\partial \varphi_i^u}{\partial y} \frac{\partial \varphi_j^u}{\partial y} \right) dxdy \qquad , r = 1,2,6$$

$$K_{ij}^{uv} = \int_{\Omega^e} \left(\left(A_{r1}A_{r2} + B_{r1}B_{r2}\right) \frac{\partial \varphi_i^u}{\partial x} \frac{\partial \varphi_j^v}{\partial y} + \left(A_{r1}A_{r6} + B_{r1}B_{r6}\right) \frac{\partial \varphi_i^u}{\partial x} \frac{\partial \varphi_j^v}{\partial x} + \right.$$

$$\left. + \left(A_{r6}A_{r2} + B_{r6}B_{r2}\right) \frac{\partial \varphi_i^u}{\partial y} \frac{\partial \varphi_j^v}{\partial y} + \left(A_{r6}^2 + B_{r6}^2\right) \frac{\partial \varphi_i^u}{\partial y} \frac{\partial \varphi_j^v}{\partial x} \right) dxdy \qquad , r = 1,2,6$$

$$K_{ij}^{u\phi_x} = \int_{\Omega^e} \left(\left(A_{r1}B_{r1} + B_{r1}D_{r1}\right) \frac{\partial \varphi_i^u}{\partial x} \frac{\partial \varphi_j^{\phi_x}}{\partial x} + \left(A_{r1}B_{r6} + B_{r1}D_{r6}\right) \frac{\partial \varphi_i^u}{\partial x} \frac{\partial \varphi_j^{\phi_x}}{\partial y} + \right.$$

$$\left. + \left(A_{r6}B_{r1} + B_{r6}D_{r1}\right) \frac{\partial \varphi_i^u}{\partial y} \frac{\partial \varphi_j^{\phi_x}}{\partial x} + \left(A_{r6}B_{r6} + B_{r6}D_{r6}\right) \frac{\partial \varphi_i^u}{\partial y} \frac{\partial \varphi_j^{\phi_x}}{\partial y} \right) dxdy \qquad , r = 1,2,6$$

$$K_{ij}^{u\phi_y} = \int_{\Omega^e} \left(\left(A_{r1}B_{r2} + B_{r1}D_{r2}\right) \frac{\partial \varphi_i^u}{\partial x} \frac{\partial \varphi_j^{\phi_y}}{\partial y} + \left(A_{r1}B_{r6} + B_{r1}D_{r6}\right) \frac{\partial \varphi_i^u}{\partial x} \frac{\partial \varphi_j^{\phi_y}}{\partial x} + \right.$$

$$\left. + \left(A_{r6}B_{r2} + B_{r6}D_{r2}\right) \frac{\partial \varphi_i^u}{\partial y} \frac{\partial \varphi_j^{\phi_y}}{\partial y} + \left(A_{r6}B_{r6} + B_{r6}D_{r6}\right) \frac{\partial \varphi_i^u}{\partial y} \frac{\partial \varphi_j^{\phi_y}}{\partial x} \right) dxdy \qquad , r = 1,2,6$$

$$K_{ij}^{uN_{xx}} = \int_{\Omega^e} \left(- A_{11} \frac{\partial \varphi_i^u}{\partial x} \varphi_j^{N_{xx}} - A_{16} \frac{\partial \varphi_i^u}{\partial y} \varphi_j^{N_{xx}} \right) dxdy$$

$$K_{ij}^{uN_{yy}} = \int_{\Omega^e} \left(- A_{12} \frac{\partial \varphi_i^u}{\partial x} \varphi_j^{N_{yy}} - A_{26} \frac{\partial \varphi_i^u}{\partial y} \varphi_j^{N_{yy}} \right) dxdy$$

$$K_{ij}^{uN_{xy}} = \int_{\Omega^e} \left(- A_{16} \frac{\partial \varphi_i^u}{\partial x} \varphi_j^{N_{xy}} - A_{66} \frac{\partial \varphi_i^u}{\partial y} \varphi_j^{N_{xy}} \right) dxdy$$

$$K_{ij}^{uM_{xx}} = \int_{\Omega^e} \left(- B_{11} \frac{\partial \varphi_i^u}{\partial x} \varphi_j^{M_{xx}} - B_{16} \frac{\partial \varphi_i^u}{\partial y} \varphi_j^{M_{xx}} \right) dxdy$$

$$K_{ij}^{uM_{yy}} = \int_{\Omega^e} \left(- B_{12} \frac{\partial \varphi_i^u}{\partial x} \varphi_j^{M_{yy}} - B_{26} \frac{\partial \varphi_i^u}{\partial y} \varphi_j^{M_{yy}} \right) dxdy$$

$$K_{ij}^{uM_{xy}} = \int_{\Omega^e} \left(- B_{16} \frac{\partial \varphi_i^u}{\partial x} \varphi_j^{M_{xy}} - B_{66} \frac{\partial \varphi_i^u}{\partial y} \varphi_j^{M_{xy}} \right) dxdy$$

$$K_{ij}^{vv} = \int_{\Omega^e} \left(\left(A_{r2}^2 + B_{r2}^2 \right) \frac{\partial \varphi_i^v}{\partial y} \frac{\partial \varphi_j^v}{\partial y} + \left(A_{r2} A_{r6} + B_{r2} B_{r6} \right) \left(\frac{\partial \varphi_i^v}{\partial y} \frac{\partial \varphi_j^v}{\partial x} + \frac{\partial \varphi_i^v}{\partial x} \frac{\partial \varphi_j^v}{\partial y} \right) + \right.$$

$$\left. + \left(A_{r6}^2 + B_{r6}^2 \right) \frac{\partial \varphi_i^v}{\partial x} \frac{\partial \varphi_j^v}{\partial x} \right) dxdy \qquad , r = 1,2,6$$

$$K_{ij}^{v\phi_x} = \int_{\Omega^e} \left(\left(A_{r2} B_{r1} + B_{r2} D_{r1} \right) \frac{\partial \varphi_i^v}{\partial y} \frac{\partial \varphi_j^{\phi_x}}{\partial x} + \left(A_{r2} B_{r6} + B_{r2} D_{r6} \right) \frac{\partial \varphi_i^v}{\partial y} \frac{\partial \varphi_j^{\phi_x}}{\partial y} + \right.$$

$$\left. + \left(A_{r6} B_{r1} + B_{r6} D_{r1} \right) \frac{\partial \varphi_i^v}{\partial x} \frac{\partial \varphi_j^{\phi_x}}{\partial x} + \left(A_{r6} B_{r6} + B_{r6} D_{r6} \right) \frac{\partial \varphi_i^v}{\partial x} \frac{\partial \varphi_j^{\phi_x}}{\partial y} \right) dxdy \qquad , r = 1,2,6$$

$$K_{ij}^{v\phi_y} = \int_{\Omega^e} \left(\left(A_{r2} B_{r2} + B_{r2} D_{r2} \right) \frac{\partial \varphi_i^v}{\partial y} \frac{\partial \varphi_j^{\phi_y}}{\partial y} + \left(A_{r2} B_{r6} + B_{r2} D_{r6} \right) \frac{\partial \varphi_i^v}{\partial y} \frac{\partial \varphi_j^{\phi_y}}{\partial x} + \right.$$

$$\left. + \left(A_{r6} B_{r2} + B_{r6} D_{r2} \right) \frac{\partial \varphi_i^v}{\partial x} \frac{\partial \varphi_j^{\phi_y}}{\partial y} + \left(A_{r6} B_{r6} + B_{r6} D_{r6} \right) \frac{\partial \varphi_i^v}{\partial x} \frac{\partial \varphi_j^{\phi_y}}{\partial x} \right) dxdy \qquad , r = 1,2,6$$

$$K_{ij}^{vN_{xx}} = \int_{\Omega^e} \left(- A_{12} \frac{\partial \varphi_i^v}{\partial y} \varphi_j^{N_{xx}} - A_{16} \frac{\partial \varphi_i^v}{\partial x} \varphi_j^{N_{xx}} \right) dxdy$$

$$K_{ij}^{vN_{yy}} = \int_{\Omega^e} \left(- A_{22} \frac{\partial \varphi_i^v}{\partial y} \varphi_j^{N_{yy}} - A_{26} \frac{\partial \varphi_i^v}{\partial x} \varphi_j^{N_{yy}} \right) dxdy$$

$$K_{ij}^{vN_{xy}} = \int_{\Omega^e} \left(- A_{26} \frac{\partial \varphi_i^v}{\partial y} \varphi_j^{N_{xy}} - A_{66} \frac{\partial \varphi_i^v}{\partial x} \varphi_j^{N_{xy}} \right) dxdy$$

$$K_{ij}^{vM_{xx}} = \int_{\Omega^e} \left(- B_{12} \frac{\partial \varphi_i^v}{\partial y} \varphi_j^{M_{xx}} - B_{16} \frac{\partial \varphi_i^v}{\partial x} \varphi_j^{M_{xx}} \right) dxdy$$

$$K_{ij}^{vM_{yy}} = \int_{\Omega^e} \left(- B_{22} \frac{\partial \varphi_i^v}{\partial y} \varphi_j^{M_{yy}} - B_{26} \frac{\partial \varphi_i^v}{\partial x} \varphi_j^{M_{yy}} \right) dxdy$$

$$K_{ij}^{vM_{xy}} = \int_{\Omega^e} \left(- B_{26} \frac{\partial \varphi_i^v}{\partial y} \varphi_j^{M_{xy}} - B_{66} \frac{\partial \varphi_i^v}{\partial x} \varphi_j^{M_{xy}} \right) dxdy$$

$$K_{ij}^{ww} = \int_{\Omega^e} \left(K^2 \left(A_{s5}^2 \right) \frac{\partial \varphi_i^w}{\partial x} \frac{\partial \varphi_j^w}{\partial x} + K^2 \left(A_{s4}^2 \right) \frac{\partial \varphi_i^w}{\partial y} \frac{\partial \varphi_j^w}{\partial y} + \right.$$

$$\left. + K^2 \left(A_{s4} A_{s5} \right) \left(\frac{\partial \varphi_i^w}{\partial x} \frac{\partial \varphi_j^w}{\partial y} + \frac{\partial \varphi_i^w}{\partial y} \frac{\partial \varphi_j^w}{\partial x} \right) \right) dxdy \qquad , s = 4,5$$

$$K_{ij}^{w\phi_x} = \int_{\Omega^e} \left(K^2 \left(A_{s5}^2\right) \frac{\partial \varphi_i^w}{\partial x} \varphi_j^{\phi_x} + K^2 \left(A_{s4} A_{s5}\right) \frac{\partial \varphi_i^w}{\partial y} \varphi_j^{\phi_x} \right) dxdy \qquad , s = 4,5$$

$$K_{ij}^{w\phi_y} = \int_{\Omega^e} \left(K^2 \left(A_{s4} A_{s5}\right) \frac{\partial \varphi_i^w}{\partial x} \varphi_j^{\phi_y} + K^2 \left(A_{s4}^2\right) \frac{\partial \varphi_i^w}{\partial y} \varphi_j^{\phi_y} \right) dxdy \qquad , s = 4,5$$

$$K_{ij}^{wQ_x} = \int_{\Omega^e} \left(- KA_{55} \frac{\partial \varphi_i^w}{\partial x} \varphi_j^{Q_x} - KA_{45} \frac{\partial \varphi_i^w}{\partial y} \varphi_j^{Q_x} \right) dxdy$$

$$K_{ij}^{wQ_y} = \int_{\Omega^e} \left(- KA_{45} \frac{\partial \varphi_i^w}{\partial x} \varphi_j^{Q_y} - KA_{44} \frac{\partial \varphi_i^w}{\partial y} \varphi_j^{Q_y} \right) dxdy$$

$$K_{ij}^{\phi_x\phi_x} = \int_{\Omega^e} \left(\left(B_{r1}^2 + D_{r1}^2\right) \frac{\partial \varphi_i^{\phi_x}}{\partial x} \frac{\partial \varphi_j^{\phi_x}}{\partial x} + \left(B_{r6}^2 + D_{r6}^2\right) \frac{\partial \varphi_i^{\phi_x}}{\partial y} \frac{\partial \varphi_j^{\phi_x}}{\partial y} + \right.$$

$$+ \left(B_{r1} B_{r6} + D_{r1} D_{r6}\right) \left(\frac{\partial \varphi_i^{\phi_x}}{\partial x} \frac{\partial \varphi_j^{\phi_x}}{\partial y} + \frac{\partial \varphi_i^{\phi_x}}{\partial y} \frac{\partial \varphi_j^{\phi_x}}{\partial x} \right) +$$

$$\left. + K^2 \left(A_{s5}^2\right) \varphi_i^{\phi_x} \varphi_j^{\phi_x} \right) dxdy \qquad , r = 1,2,6 \quad , s = 4,5$$

$$K_{ij}^{\phi_x\phi_y} = \int_{\Omega^e} \left(\left(B_{r1} B_{r2} + D_{r1} D_{r2}\right) \frac{\partial \varphi_i^{\phi_x}}{\partial x} \frac{\partial \varphi_j^{\phi_y}}{\partial y} + \left(B_{r1} B_{r6} + D_{r1} D_{r6}\right) \frac{\partial \varphi_i^{\phi_x}}{\partial x} \frac{\partial \varphi_j^{\phi_y}}{\partial x} + \right.$$

$$+ \left(B_{r6} B_{r2} + D_{r6} D_{r2}\right) \frac{\partial \varphi_i^{\phi_x}}{\partial y} \frac{\partial \varphi_j^{\phi_y}}{\partial y} + \left(B_{r6}^2 + D_{r6}^2\right) \frac{\partial \varphi_i^{\phi_x}}{\partial y} \frac{\partial \varphi_j^{\phi_y}}{\partial x} +$$

$$\left. + K^2 \left(A_{s4} A_{s5}\right) \varphi_i^{\phi_x} \varphi_j^{\phi_y} \right) dxdy \qquad , r = 1,2,6 \quad , s = 4,5$$

$$K_{ij}^{\phi_x N_{xx}} = \int_{\Omega^e} \left(- B_{11} \frac{\partial \varphi_i^{\phi_x}}{\partial x} \varphi_j^{N_{xx}} - B_{16} \frac{\partial \varphi_i^{\phi_x}}{\partial y} \varphi_j^{N_{xx}} \right) dxdy$$

$$K_{ij}^{\phi_x N_{yy}} = \int_{\Omega^e} \left(- B_{12} \frac{\partial \varphi_i^{\phi_x}}{\partial x} \varphi_j^{N_{yy}} - B_{26} \frac{\partial \varphi_i^{\phi_x}}{\partial y} \varphi_j^{N_{yy}} \right) dxdy$$

$$K_{ij}^{\phi_x N_{xy}} = \int_{\Omega^e} \left(- B_{16} \frac{\partial \varphi_i^{\phi_x}}{\partial x} \varphi_j^{N_{xy}} - B_{66} \frac{\partial \varphi_i^{\phi_x}}{\partial y} \varphi_j^{N_{xy}} \right) dxdy$$

$$K_{ij}^{\phi_x M_{xx}} = \int_{\Omega^e} \left(- D_{11} \frac{\partial \varphi_i^{\phi_x}}{\partial x} \varphi_j^{M_{xx}} - D_{16} \frac{\partial \varphi_i^{\phi_x}}{\partial y} \varphi_j^{M_{xx}} \right) dxdy$$

$$K_{ij}^{\phi_x M_{yy}} = \int_{\Omega^e} \left(- D_{12} \frac{\partial \varphi_i^{\phi_x}}{\partial x} \varphi_j^{M_{yy}} - D_{26} \frac{\partial \varphi_i^{\phi_x}}{\partial y} \varphi_j^{M_{yy}} \right) dxdy$$

$$K_{ij}^{\phi_x M_{xy}} = \int_{\Omega^e} \left(- D_{16} \frac{\partial \varphi_i^{\phi_x}}{\partial x} \varphi_j^{M_{xy}} - D_{66} \frac{\partial \varphi_i^{\phi_x}}{\partial y} \varphi_j^{M_{xy}} \right) dxdy$$

$$K_{ij}^{\phi_x Q_x} = \int_{\Omega^e} \left(- KA_{55} \varphi_i^{\phi_x} \varphi_j^{Q_x} \right) dxdy$$

$$K_{ij}^{\phi_x Q_y} = \int_{\Omega^e} \left(- KA_{45} \varphi_i^{\phi_x} \varphi_j^{Q_y} \right) dxdy$$

$$K_{ij}^{\phi_y \phi_y} = \int_{\Omega^e} \left(\left(B_{r2}^2 + D_{r2}^2 \right) \frac{\partial \varphi_i^{\phi_y}}{\partial y} \frac{\partial \varphi_j^{\phi_y}}{\partial y} + \left(B_{r6}^2 + D_{r6}^2 \right) \frac{\partial \varphi_i^{\phi_y}}{\partial x} \frac{\partial \varphi_j^{\phi_y}}{\partial x} + \right.$$

$$+ \left(B_{r2} B_{r6} + D_{r2} D_{r6} \right) \left(\frac{\partial \varphi_i^{\phi_y}}{\partial y} \frac{\partial \varphi_j^{\phi_y}}{\partial x} + \frac{\partial \varphi_i^{\phi_y}}{\partial x} \frac{\partial \varphi_j^{\phi_y}}{\partial y} \right) +$$

$$\left. + K^2 \left(A_{s4}^2 \right) \varphi_i^{\phi_y} \varphi_j^{\phi_y} \right) dxdy \qquad , r = 1,2,6 \quad , s = 4,5$$

$$K_{ij}^{\phi_y N_{xx}} = \int_{\Omega^e} \left(- B_{12} \frac{\partial \varphi_i^{\phi_y}}{\partial y} \varphi_j^{N_{xx}} - B_{16} \frac{\partial \varphi_i^{\phi_y}}{\partial x} \varphi_j^{N_{xx}} \right) dxdy$$

$$K_{ij}^{\phi_y N_{yy}} = \int_{\Omega^e} \left(- B_{22} \frac{\partial \varphi_i^{\phi_y}}{\partial y} \varphi_j^{N_{yy}} - B_{26} \frac{\partial \varphi_i^{\phi_y}}{\partial x} \varphi_j^{N_{yy}} \right) dxdy$$

$$K_{ij}^{\phi_y N_{xy}} = \int_{\Omega^e} \left(- B_{26} \frac{\partial \varphi_i^{\phi_y}}{\partial y} \varphi_j^{N_{xy}} - B_{66} \frac{\partial \varphi_i^{\phi_y}}{\partial x} \varphi_j^{N_{xy}} \right) dxdy$$

$$K_{ij}^{\phi_y M_{xx}} = \int_{\Omega^e} \left(- D_{12} \frac{\partial \varphi_i^{\phi_y}}{\partial y} \varphi_j^{M_{xx}} - D_{16} \frac{\partial \varphi_i^{\phi_y}}{\partial x} \varphi_j^{M_{xx}} \right) dxdy$$

$$K_{ij}^{\phi_y M_{yy}} = \int_{\Omega^e} \left(- D_{22} \frac{\partial \varphi_i^{\phi_y}}{\partial y} \varphi_j^{M_{yy}} - D_{26} \frac{\partial \varphi_i^{\phi_y}}{\partial x} \varphi_j^{M_{yy}} \right) dxdy$$

$$K_{ij}^{\phi_y M_{xy}} = \int_{\Omega^e} \left(- D_{26} \frac{\partial \varphi_i^{\phi_y}}{\partial y} \varphi_j^{M_{xy}} - D_{66} \frac{\partial \varphi_i^{\phi_y}}{\partial x} \varphi_j^{M_{xy}} \right) dxdy$$

$$K_{ij}^{\phi_y Q_x} = \int_{\Omega^e} \left(- KA_{45} \varphi_i^{\phi_y} \varphi_j^{Q_x} \right) dxdy$$

$$K_{ij}^{\phi_y Q_y} = \int_{\Omega^e} \left(- KA_{44} \varphi_i^{\phi_y} \varphi_j^{Q_y} \right) dxdy$$

$$K_{ij}^{N_{xx} N_{xx}} = \int_{\Omega^e} \left(\frac{\partial \varphi_i^{N_{xx}}}{\partial x} \frac{\partial \varphi_j^{N_{xx}}}{\partial x} + \varphi_i^{N_{xx}} \varphi_j^{N_{xx}} \right) dxdy$$

$$K_{ij}^{N_{xx} N_{xy}} = \int_{\Omega^e} \left(\frac{\partial \varphi_i^{N_{xx}}}{\partial x} \frac{\partial \varphi_j^{N_{xy}}}{\partial y} \right) dxdy$$

$$K_{ij}^{N_{yy} N_{yy}} = \int_{\Omega^e} \left(\frac{\partial \varphi_i^{N_{yy}}}{\partial y} \frac{\partial \varphi_j^{N_{yy}}}{\partial y} + \varphi_i^{N_{yy}} \varphi_j^{N_{yy}} \right) dxdy$$

$$K_{ij}^{N_{yy} N_{xy}} = \int_{\Omega^e} \left(\frac{\partial \varphi_i^{N_{yy}}}{\partial y} \frac{\partial \varphi_j^{N_{xy}}}{\partial x} \right) dxdy$$

$$K_{ij}^{N_{xy}N_{xy}} = \int_{\Omega^e} \left(\frac{\partial \varphi_i^{N_{xy}}}{\partial x} \frac{\partial \varphi_j^{N_{xy}}}{\partial x} + \frac{\partial \varphi_i^{N_{xy}}}{\partial y} \frac{\partial \varphi_j^{N_{xy}}}{\partial y} + \varphi_i^{N_{xy}} \varphi_j^{N_{xy}} \right) dxdy$$

$$K_{ij}^{M_{xx}M_{xx}} = \int_{\Omega^e} \left(\frac{\partial \varphi_i^{M_{xx}}}{\partial x} \frac{\partial \varphi_j^{M_{xx}}}{\partial x} + \varphi_i^{M_{xx}} \varphi_j^{M_{xx}} \right) dxdy$$

$$K_{ij}^{M_{xx}M_{xy}} = \int_{\Omega^e} \left(\frac{\partial \varphi_i^{M_{xx}}}{\partial x} \frac{\partial \varphi_j^{M_{xy}}}{\partial y} \right) dxdy$$

$$K_{ij}^{M_{xx}Q_x} = \int_{\Omega^e} \left(-\frac{\partial \varphi_i^{M_{xx}}}{\partial x} \varphi_j^{Q_x} \right) dxdy$$

$$K_{ij}^{M_{yy}M_{yy}} = \int_{\Omega^e} \left(\frac{\partial \varphi_i^{M_{yy}}}{\partial y} \frac{\partial \varphi_j^{M_{yy}}}{\partial y} + \varphi_i^{M_{yy}} \varphi_j^{M_{yy}} \right) dxdy$$

$$K_{ij}^{M_{yy}M_{xy}} = \int_{\Omega^e} \left(\frac{\partial \varphi_i^{M_{yy}}}{\partial y} \frac{\partial \varphi_j^{M_{xy}}}{\partial x} \right) dxdy$$

$$K_{ij}^{M_{yy}Q_y} = \int_{\Omega^e} \left(-\frac{\partial \varphi_i^{M_{yy}}}{\partial y} \varphi_j^{Q_y} \right) dxdy$$

$$K_{ij}^{M_{xy}M_{xy}} = \int_{\Omega^e} \left(\frac{\partial \varphi_i^{M_{xy}}}{\partial x} \frac{\partial \varphi_j^{M_{xy}}}{\partial x} + \frac{\partial \varphi_i^{M_{xy}}}{\partial y} \frac{\partial \varphi_j^{M_{xy}}}{\partial y} + \varphi_i^{M_{xy}} \varphi_j^{M_{xy}} \right) dxdy$$

$$K_{ij}^{M_{xy}Q_x} = \int_{\Omega^e} \left(-\frac{\partial \varphi_i^{M_{xy}}}{\partial y} \varphi_j^{Q_x} \right) dxdy$$

$$K_{ij}^{M_{xy}Q_y} = \int_{\Omega^e} \left(-\frac{\partial \varphi_i^{M_{xy}}}{\partial x} \varphi_j^{Q_y} \right) dxdy$$

$$K_{ij}^{Q_xQ_x} = \int_{\Omega^e} \left(\frac{\partial \varphi_i^{Q_x}}{\partial x} \frac{\partial \varphi_j^{Q_x}}{\partial x} + 2\varphi_i^{Q_x} \varphi_j^{Q_x} \right) dxdy$$

$$K_{ij}^{Q_xQ_y} = \int_{\Omega^e} \left(\frac{\partial \varphi_i^{Q_x}}{\partial x} \frac{\partial \varphi_j^{Q_y}}{\partial y} \right) dxdy$$

$$K_{ij}^{Q_yQ_y} = \int_{\Omega^e} \left(\frac{\partial \varphi_i^{Q_y}}{\partial y} \frac{\partial \varphi_j^{Q_y}}{\partial y} + 2\varphi_i^{Q_y} \varphi_j^{Q_y} \right) dxdy$$

$$C_{ij}^{uN_{xx}} = \int_{\Omega^e} \left(I_0 \varphi_i^u \frac{\partial \varphi_j^{N_{xx}}}{\partial x} \right) dxdy$$

$$C_{ij}^{uN_{xy}} = \int_{\Omega^e} \left(I_0 \varphi_i^u \frac{\partial \varphi_j^{N_{xy}}}{\partial y} \right) dxdy$$

$$C_{ij}^{uM_{xx}} = \int_{\Omega^e} \left(I_1 \varphi_i^u \frac{\partial \varphi_j^{M_{xx}}}{\partial x} \right) dxdy$$

$$C_{ij}^{uM_{xy}} = \int_{\Omega^e} \left(I_1 \varphi_i^u \frac{\partial \varphi_j^{M_{xy}}}{\partial y} \right) dxdy$$

$$C_{ij}^{uQ_x} = \int_{\Omega^e} \left(-I_1 \varphi_i^u \varphi_j^{Q_x} \right) dxdy$$

$$C_{ij}^{vN_{yy}} = \int_{\Omega^e} \left(I_0 \varphi_i^v \frac{\partial \varphi_j^{N_{yy}}}{\partial y} \right) dxdy$$

$$C_{ij}^{vN_{xy}} = \int_{\Omega^e} \left(I_0 \varphi_i^v \frac{\partial \varphi_j^{N_{xy}}}{\partial x} \right) dxdy$$

$$C_{ij}^{vM_{yy}} = \int_{\Omega^e} \left(I_1 \varphi_i^v \frac{\partial \varphi_j^{M_{yy}}}{\partial y} \right) dxdy$$

$$C_{ij}^{vM_{xy}} = \int_{\Omega^e} \left(I_1 \varphi_i^v \frac{\partial \varphi_j^{M_{xy}}}{\partial x} \right) dxdy$$

$$C_{ij}^{vQ_y} = \int_{\Omega^e} \left(-I_1 \varphi_i^v \varphi_j^{Q_y} \right) dxdy$$

$$C_{ij}^{wQ_x} = \int_{\Omega^e} \left(I_0 \varphi_i^w \frac{\partial \varphi_j^{Q_x}}{\partial x} \right) dxdy$$

$$C_{ij}^{wQ_y} = \int_{\Omega^e} \left(I_0 \varphi_i^w \frac{\partial \varphi_j^{Q_y}}{\partial y} \right) dxdy$$

$$C_{ij}^{\phi_x N_{xx}} = \int_{\Omega^e} \left(I_1 \varphi_i^{\phi_x} \frac{\partial \varphi_j^{N_{xx}}}{\partial x} \right) dxdy$$

$$C_{ij}^{\phi_x N_{xy}} = \int_{\Omega^e} \left(I_1 \varphi_i^{\phi_x} \frac{\partial \varphi_j^{N_{xy}}}{\partial y} \right) dxdy$$

$$C_{ij}^{\phi_x M_{xx}} = \int_{\Omega^e} \left(I_2 \varphi_i^{\phi_x} \frac{\partial \varphi_j^{M_{xx}}}{\partial x} \right) dxdy$$

$$C_{ij}^{\phi_x M_{xy}} = \int_{\Omega^e} \left(I_2 \varphi_i^{\phi_x} \frac{\partial \varphi_j^{M_{xy}}}{\partial y} \right) dxdy$$

$$C_{ij}^{\phi_x Q_x} = \int_{\Omega^e} \left(-I_2 \varphi_i^{\phi_x} \varphi_j^{Q_x} \right) dxdy$$

$$C_{ij}^{\phi_y N_{yy}} = \int_{\Omega^e} \left(I_1 \varphi_i^{\phi_y} \frac{\partial \varphi_j^{N_{yy}}}{\partial y} \right) dxdy$$

$$C_{ij}^{\phi_y N_{xy}} = \int_{\Omega^e} \left(I_1 \varphi_i^{\phi_y} \frac{\partial \varphi_j^{N_{xy}}}{\partial x} \right) dxdy$$

$$C_{ij}^{\phi_y M_{yy}} = \int_{\Omega^e} \left(I_2 \varphi_i^{\phi_y} \frac{\partial \varphi_j^{M_{yy}}}{\partial y} \right) dxdy$$

$$C_{ij}^{\phi_y M_{xy}} = \int_{\Omega^e} \left(I_2 \varphi_i^{\phi_y} \frac{\partial \varphi_j^{M_{xy}}}{\partial x} \right) dxdy$$

$$C_{ij}^{\phi_y Q_y} = \int_{\Omega^e} \left(-I_2 \varphi_i^{\phi_y} \varphi_j^{Q_y} \right) dxdy$$

$$M_{ij}^{uu} = \int_{\Omega^e} \left(\left(I_0^2 + I_1^2 \right) \varphi_i^u \varphi_j^u \right) dxdy$$

$$M_{ij}^{u\phi_x} = \int_{\Omega^e} \left(\left(I_0 I_1 + I_1 I_2 \right) \varphi_i^u \varphi_j^{\phi_x} \right) dxdy$$

$$M_{ij}^{vv} = \int_{\Omega^e} \left(\left(I_0^2 + I_1^2 \right) \varphi_i^v \varphi_j^v \right) dxdy$$

$$M_{ij}^{v\phi_y} = \int_{\Omega^e} \left(\left(I_0 I_1 + I_1 I_2 \right) \varphi_i^v \varphi_j^{\phi_y} \right) dxdy$$

$$M_{ij}^{ww} = \int_{\Omega^e} \left(I_0^2 \varphi_i^w \varphi_j^w \right) dxdy$$

$$M_{ij}^{\phi_x \phi_x} = \int_{\Omega^e} \left(\left(I_1^2 + I_2^2 \right) \varphi_i^{\phi_x} \varphi_j^{\phi_x} \right) dxdy$$

$$M_{ij}^{\phi_y \phi_y} = \int_{\Omega^e} \left(\left(I_1^2 + I_2^2 \right) \varphi_i^{\phi_y} \varphi_j^{\phi_y} \right) dxdy$$

$$F_i^{Q_x} = \int_{\Omega^e} \left(-\frac{\partial \varphi_i^{Q_x}}{\partial x} q(x,y) \right) dxdy$$

$$F_i^{Q_y} = \int_{\Omega^e} \left(-\frac{\partial \varphi_i^{Q_y}}{\partial y} q(x,y) \right) dxdy$$

These integral expressions make use of the symmetry in the laminate stiffnesses, namely, $A_{ij} = A_{ji}$, $B_{ij} = B_{ji}$ and $D_{ij} = D_{ji}$. In addition, for any submatrice relating two given variables (*a* and *b*) the following relations hold, $K_{ij}^{ab} = K_{ji}^{ba}$, $C_{ij}^{ab} = C_{ji}^{ba}$ and $M_{ij}^{ab} = M_{ji}^{ba}$, which renders symmetry to the all finite element matrices.

2.9 References

[1] Carrera, E., Theories and finite elements for multilayered, anisotropic, composite plates and shells, *Archives of Computational Methods in Engineering*, Vol. 9(2), pp. 87-140, 2002.

[2] Reddy, J.N. and Robbins Jr, D.H., Theories and computational models for composite laminates, *Applied Mechanics Reviews*, Vol. 47(6), pp. 147-169, 1994.

[3] Noor, A.K. and Burton, W.S., Assessment of shear deformation theories for multilayered composite plates, *Applied Mechanics Reviews*, Vol. 42(1), pp. 1-13, 1989.

[4] Washizu K., *Variational Methods in Elasticity and Plasticity*, Pergamon Press, New York, 1975.

[5] Reddy, J.N., *Energy Principles and Variational Methods in Applied Mechanics*, Wiley, New York, 2002.

[6] Reddy, J.N., *An Introduction to the Finite Element Method*, 3rd ed., McGraw-Hill, New York, 2006.

[7] Reddy, J.N., *Mechanics of Laminated Composite Plates and Shells: Theory and Analysis*, 2nd ed., CRC Press, Boca Raton, 2004.

[8] Pontaza, J.P. and Reddy, J.N., Mixed plate bending elements based on least-squares formulation, *International Journal for Numerical Methods in Engineering*, vol. 60, pp. 891-922, 2004.

[9] Pontaza, J.P., Least-squares variational principles and the finite element method: theory, formulations, and models for solid and fluid mechanics, *Finite Elements in Analysis and Design*, vol. 41, pp. 703-728, 2005.

[10] Duan, H.-Y. and Lin, Q., Mixed finite elements of least-squares type for elasticity, *Computer Methods in Applied Mechanics and Engineering*, vol. 194, pp. 1093-1112, 2005.

[11] Reissner, E., On a certain mixed variational theory and a proposed application, *International Journal for Numerical Methods in Engineering*, vol. 20, pp. 1366-1368, 1984.

[12] Reissner, E., On a mixed variational theorem and on a shear deformable plate theory, *International Journal for Numerical Methods in Engineering*, vol. 23, pp. 193-198, 1986.

[13] Duan, H.-Y. and Liang, G.-P., Mixed and nonconforming finite element approximations of Reissner-Mindlin plates, *Computer Methods in Applied Mechanics and Engineering*, vol. 192, pp. 5265-5281, 2003.

[14] Warburton, T.C., Sherwin, S.J. and Karniadakis, G.E., Basis functions for triangular and quadrilateral high-order elements, *SIAM Journal on Scientific Computing*, vol. 20(5), pp. 1671-1695, 1999.

[15] Bai, Z., Demmel, J., Dongarra, J., Ruhe, A. and Vorst, H., *Templates for the Solution of Algebraic Eigenvalue Problems: A Practical Guide*, SIAM, Philadelphia, 2000.

REPORT DOCUMENTATION PAGE

Form Approved
OMB NO. 0704-0188

1. AGENCY USE ONLY (Leave Blank)	2. REPORT DATE	3. REPORT TYPE AND DATES COVERED
	May 2008	Final Report (March 2005-March 2008)

4. TITLE AND SUBTITLE

A NEW COMPUTATIONAL METHODOLOGY FOR STRUCTURAL DYNAMICS PROBLEMS

5. FUNDING NUMBERS

ARO Grant W911NF-05-1-0122
AMSRD-ARL-RO-OI Proposal Number: 45508-EG

6. AUTHOR(S)
J. N. Reddy

7. PERFORMING ORGANIZATION NAME(S) AND ADDRESS(ES)
Department of Mechanical Engineering,
Texas A&M University
College Station, Texas 77843-3123

8. PERFORMING ORGANIZATION REPORT NUMBER

9. SPONSORING / MONITORING AGENCY NAME(S) AND ADDRESS(ES)

U. S. Army Research Office
P.O. Box 12211
Research Triangle Park, NC 27709-2211

10. SPONSORING / MONITORING AGENCY REPORT NUMBER

11. SUPPLEMENTARY NOTES

The views, opinions and/or findings contained in this report are those of the author(s) and should not be construed as an official Department of the Army position, policy or decision, unless so designated by the documentation.

12 a. DISTRIBUTION / AVAILABILITY STATEMENT

12 b. DISTRIBUTION CODE

13. ABSTRACT (Maximum 200 words)

Most structural components encountered in army vehicles and armor can be classified as beams, plates, or shells for analysis purposes. While these structural elements are designed to function properly under thermo-mechanical loads encountered in their use, they do develop high stresses and experience high vibration frequencies that may make them non-functional in actual service conditions. The objective of this research is to develop consistent plate and shell theories and associated computational framework for linear and non-linear problems of structural dynamics in which localized high gradients of the solutions are resolved accurately. Crucial importance of this framework will be demonstrated computationally through well known benchmark model problems in the area of solid mechanics with special focus on composite plate and shell structures. The developed methodology and has applications to solid and structural mechanics problems and it will provide highly reliable, robust and accurate computational technology to the United States Army Laboratories. The specific objectives of this research were to (1) develop accurate and consistent structural theories and associated finite element models of plates and shells that account for transverse shear deformation and illustrate the accuracy using benchmark plate and shell problems; (2) develop mixed and least-squares finite element models of the refined theories for the analysis of plates and shells; and (3) incorporate geometric nonlinearity into the mixed and least-squares finite element models and study problems of plates and shells.

14. SUBJECT TERMS

laminated composite plates and shells, least-squares finite element models, layerwise theory, third-order shear deformation theory, bending, buckling and vibration response

15. NUMBER OF PAGES
56 including cover page

16. PRICE CODE

17. SECURITY CLASSIFICATION OR REPORT	18. SECURITY CLASSIFICATION ON THIS PAGE	19. SECURITY CLASSIFICATION OF ABSTRACT	20. LIMITATION OF ABSTRACT
UNCLASSIFIED	**UNCLASSIFIED**	**UNCLASSIFIED**	**UL**

REPORT DOCUMENTATION PAGE (SF298)
(Continuation Sheet)

1. LIST OF JOURNAL PAPERS PUBLISHED

- J.N. Reddy and R. A. Arciniega, "Mechanical and Thermal Buckling of Ceramic-Metal Plates," Chapter 6 in *Analysis and Design of Plated Structures*, *Statics*, N. E. Shanmugam and C. M. Wang (eds), Wood-Head Publishing, Oxford, UK, pp. 138-160, 2005.
- R. A. Arciniega and J. N. Reddy, "A Consistent Third-Order Shell Theory with Application to Bending of Laminated Composite Cylindrical Shells," *AIAA Journal,* Vol. 43, No. 9, pp. 2024-2038, 2005.
- V. Prabhakar and J. N. Reddy, "Spectral/*hp* Penalty Least-Squares Finite Element Formulation for the Steady Incompressible Navier-Stokes Equations," *Journal of Computational Physics*, Vol. 215, No. 1, pp. 274-297, 2006.
- J.N. Reddy and R. A. Arciniega, "Vibration of Functionally Graded Ceramic-Metal Plates," in *Analysis and Design of Plated Structures: Dynamics*, N. E. Shanmugam and C. M. Wang (eds), Wood-Head Publishing, Oxford, UK, pp. 293-321, 2007.
- R. A. Arciniega and J. N. Reddy, "Tensor-based Finite Element Formulation for Geometrically Nonlinear Analysis of Shell Structures," *Computer Methods in Applied Mechanics and Engineering,* Vol. 196, Nos. 4-6, pp. 1048-1073, 2007.
- R. A. Arciniega and J. N. Reddy, "Large deformation analysis of functionally graded shells," *International Journal of Solids and Structures,* Vol. 44, pp. 2036-2052, 2007.
- V. Prabhakar and J. N. Reddy, "A Stress-based Least-Squares Finite-element model for Incompressible Navier-Stokes Equations," *International Journal for Numerical Methods in Fluids*, vol. 54, issue 11, pp. 1369-1385, 2007.
- F. Moleir, C.M. Mota Soares, C.A. Mota Soares, and J.N. Reddy, "Mixed least-squares finite element model for the static analysis of laminated composite plates," *Computers and Structures,* Vol. 86 pp. 826–838, 2008.
- Henrique Santos, C. M. Mota Soares, C. A. Mota Soares, and J.N. Reddy, "A finite element model for the analysis of 3D axisymmetric laminated shells with piezoelectric sensors and actuators: Bending and free vibrations," *Computers and Structures,* Vol. 86 pp. 940–947, 2008.

2. SCIENTIFIC PERSONNEL and HONORS AND AWARDS

- J. N. Reddy, Roman Arciniega, V. Prabhakar, Filipa Moleiro, Yetzirah Urthaler
- *Editor-in-Chief*, Applied Mechanics Reviews, American Society of Mechanical Engineers, New York, October 2007.
- *Fellow* of the American Institute of Aeronautics and Astronautics, May 2005.
- *Distinguished Achievement in Teaching* Award, Association of Former Students (AFS), Texas A&M University, 2007 (university level).
- *Distinguished Lecture* of the Sigma Xi, Texas A&M University, October 2005.
- *Distinguished Research Award* of the Sigma Xi, Texas A&M University, March 2005.

- *Presented the following key note lectures:*
  - "Computational Modeling of Materials and Structures and New Computational Methodology," The *US-Africa Workshop on Mechanics and Materials,* University of Cape Town, South Africa, January 23-28, 2005.
  - "A Finite Deformation Shell Formulation for the Analysis of Composite and Functionally Graded Material Structures," *Symposium on Physics and Mechanics of Advanced Materials*, January 18-20, 2006, Singapore.
  - "On Nonlinear Analysis of Composite and Functionally Graded Shell Structures," *Tenth East Asia Pacific Conference on Structural Engineering and Construction*, August 2-4, 2006, Bangkok, Thailand.
  - "Nonlinear Analysis of Composite and FGM Shell Structures Using Tensor-Based Shell Elements," *International Workshop in Mechanics of Composites*, Bad Herrenab, Germany, November 26-29, 2006.

3. INVENTIONS None

4. SCIENTIFIC PROGRESS AND ACCOMPLISHMENTS

A tensor-oriented finite element formulation is developed by using curvilinear coordinates. High-order elements with Lagrangian interpolations are used to avoid membrane and shear locking. The formulation is based on the first-order shell theory with seven parameters with exact nonlinear deformations and under the framework of the Lagrangian description. Numerical results of the present formulation for typical benchmark with applications to laminated composite shells and functionally graded shells were carried out. Least-squares based finite element models of viscous incompressible flows are also developed with the interest to formulate computational procedures for fluid-structure interaction problems. Finally, mixed finite element models of laminated composite plates were also developed that allow accurate computation of stress resultants. In summary, the folowing accomplishments are reported:

1. The theoretical as well as finite element formulation of unified, consistent, nonlinear shell theory that accounts for large displacements, large rotations and moderately large strains was developed. The computational model is used to analyze (a) laminated composite shells and (b) two-phase functionally graded shells. The applicability of the finite element model to a variety of geometrically complex shells is demonstrated with a a number of benchmark problems of isotropic, laminated composite (cross-ply, angle-ply, and general laminated) shells.
2. Least-squares finite element models of viscous incompressible fluids are developed. The models are characterized by positive-definite system of equations that can be solved using iterative methods.
3. Mixed finite element models of laminated plates in which the generalized displacements and stress resultants are approximated independently are developed.

5. TECHNOLOGY TRANSFER

The PI is in continuous contact with Mr. Rostam-Abadi of TACOM and Drs. A.M. Rajendran and Bruce LaMattina of ARO concerning the results of this research. He has visited both TACOM in Warren and ARO in Research Triangle Park to present the scientific progress made.